Markus Sommerfeld
Institute for Integrated Energy Systems
University of Victoria
3800 Finnerty Rd
Victoria, BC, Canada
V8P 5C2

June 28, 2019

Revision to wes-2019-7: Improving mid-altitude mesoscale wind speed forecasts using LiDAR-based observation nudging for Airborne Wind Energy Systems

Dear Dr. Floors,

Thank you very much for your helpful review of our manuscript, "Improving mid-altitude mesoscale wind speed forecasts using LiDAR-based observation nudging for Airborne Wind Energy Systems", wes-2019-7. We have modified the manuscript accordingly, removed or consolidated several figures and adapted the text.

Please find our response to individual comments below.

Changes are highlighted in the "Supplementary Material" pdf. Text and figures marked in red were removed from the original submission and replaced by text and figures marked in blue. Following are our replies to your comments and a description of modification to the manuscript.

Sincerely,
Markus Sommerfeld

Comments by the Referee

I. General comments

The paper is a useful contribution to a better understanding of the winds at larger heights, which is not only relevant for the AWES applications for which the paper is written, but also in general for large wind turbines. Nudging with wind observations within the

boundary layer has not been done a lot, so it is interesting to see how the WRF model behaves. I have two major issues with the paper:

1. *In the abstract it is stated that: "Observation nudging improves the overall accuracy of WRF". This cannot be concluded based on this study, because the observations are assimilated and then also used for evaluation. This will obviously result in the model being closer to the measurements, but this has nothing to do with WRF being more accurate 'overall'. If you want to draw this conclusion you would have to compare with measurements that are not assimilated in the model, preferably at some distance away from the point where the observations are nudged. Otherwise it should be more clearly written that the nudging is only valid at the lidar point: as it can be seen from Fig. 6 the modelled wind speed is just bias-corrected with approx. 1 m/s over a 180 km area, but it might well be that this detoriates wind speed comparison at other locations. For example, it could be that the bias at this point is caused by a wrong surface roughness or other local flow properties, which means the bias does not exists in other places. Also the nudging is likely only valid over land, because over sea the physical processes that determine the wind profile at a given time are different. All this should be written more clearly throughout the abstract/results/discussion/conclusion. Figures 2-6 all show the same message: nudging brings the model closer to the observations, so they can be combined into one or perhaps two figures. Figure 11 and 12 also show the same thing and can be combined.*

   - The sentence in the abstract has been changed to a more precise formulation: 'Observation nudging improves the WRF accuracy at the measurement location.'
   - Wind conditions and WRF simulation offshore are not subject of this manuscript and no investigation of observation nudging offshore have been performed. While we assume that the non-physical nature of observation nudging impacts the flow offshore as well, we can not draw this conclusion at. We therefore would prefer not mentioning offshore conditions in this paper.
   - While figure 2-6 all show the impact of observation nudging, they present different aspects. Figure 2 visualizes the correlation between measurements and absolute occurrence of certain wind conditions, figure 3 shows the overall altitude dependent impact of nudging, figure 4 shows a representative day and figure 5 and 6 shows the spatial impact of observation nudging. We see that figure 5 and 6 show similar results and chose to remove figure 6.
   - Figure 11 shows the mean wind speed profiles categorized based on Obukhov length whereas figure 12 shows the purely mathematical k-means clustered wind speed profile probability distribution. This mathematical approach was chosen due to the lack of heat flux and temperature measurements and to be consistent with "LiDAR-based characterization of mid-altitude wind conditions for airborne wind energy systems" doi: 10.1002/we.2343. Since the

WRF simulations provide all this information we decided to represent the Obukhov length categorized data in the same way as the k-means clustered data previously.

2. *The definition of the Obukhov length in Eq. 4 is not clear or wrong: to classify stability one should take into account the effect of the *virtual* kinematic sensible heat flux and not the dynamic sensible heat flux directly from WRF (W/m2), which seems to be implied in Eq. 4 (although Hsfc is not defined anywhere). In the WRF model surface layer fluxes are split up in a sensible and latent heat flux. Sensible and latent heat flux are equally important in a fairly moist areas as Germany (see for example Stull (2017) or Floors et al. (2013)), so they should both be used when computing the Obukhov length.*

   - We adjusted our calculation of the Obukhov length in equation 4. The equation, which was taken from Sempreviva and Gryning, 1996 "Humidity fluctuations in the marine boundary layer measured at a coastal site with an infrared humidity sensor", now takes latent and sensible surface heat flux into account.
   - $OL = \left(\frac{-u_*^3 \theta_v}{kg}\right)\left(\frac{1}{Q_S} + \frac{0.61}{Q_L \theta}\right)$
   - Equation 18.16 just uses the kinematic surface heat flux in Stull,2017: Practical Meteorology An Algebra-based Survey of Atmospheric Science

II. Specific comments

- *p3l8: It would be useful to give the opening angle of the lidar.*
  - Added the opening angle in brackets: 62 degree or 28 degree to the horizon.
- *p4l2: What CNR threshold is used for filtering the data? What is the definition of an 'available' measurement?*
  - We used a self-defined filter described in the "LiDAR-based characterization of mid-altitude wind conditions for airborne wind energy systems" doi: 10.1002/we.2343. We added a short description in this manuscript and refer to the previously mentioned paper for detailed information. Data availability is defined as the time when useful data (not filtered out) is available divided by the total time of the measurement period (6 months).
- *p4l6-9: I would remove this, because it has nothing to with the measurements, which is what the section is about. It is also discussing some of the results which have not yet been presented.*
  - Agreed and removed.
- *p4l13-17: All brackets make this section difficult to read. Please rewrite.*

- Removing these brackets is difficult as some of them are due to the bibliography style, reference to figures and the definition of new abbreviations.Rewrote the definition of NoOBS and OBS in a sub-clause and removed the brackets around the WRF version.

- *p4: Please mention the land-surface, radiation and surface-layer scheme that were used in the WRF model.*
  - land-surface option: sf_surface_physics: 4, Noah-MP land-surface model (see additional &noah_mp namelist)
  - long wave: ra_lw_physics: 1, rrtm scheme
  - short wave: ra_sw_physics: 1, Dudhia scheme
  - radt: 18,6,2 min between physics calls
  - surface-layer option: sf_sfclay_physics: 5, MYNN surface layer
  - reference: `https://esrl.noaa.gov/gsd/wrfportal/namelist_input_options.html`

- *p6l2: 180 km is a very large distance. See major comment 1.*
  - The radius of 180 km is chosen so that the entire inner domain is affected by obs nudging and the spatial impact can be quantified.
  - changed subsentence to:"... thereby affecting the whole inner domain."

- *p7l2: I assume the wind direction is not calculated like this because it would lead to discontinuities when crossing 360 degrees. Please add more details.*
  - Angular difference is calculated by using *angdiff* in Matlab. The results are wrapped on the interval $[-\pi,\pi]$. Added a sub-clause to this point.

- *Section 4.1-4.3: see major comment 1;*
  - See response to comment 1.

- *p14l10-12: I think this is an important conclusion from this work and I agree that this is a potential application of using nudged WRF simulations. Perhaps it is useful to relate this to the discussion in Gryning et al. (2019) regarding the wind speed bias from lidars as a function of CNR threshold and data availability, to show that this issue is not specific for the site studied in your paper.*
  - Added this reference. We agree that it is good to point out that this is not a site specific issue.
  - Added to conclusion:
    * The bias between real and LiDAR measured wind speed, which depends on the applied CNR threshold and data availability, can result in a misrepresentation of the actual wind conditions especially at higher altitudes. Mesoscale models, particularly with observation nudging, can be used to account for this error.

- *p16l9-11: The wind speed in summer is mostly lower due to the lower synoptic pressure gradients in that time of the year, not so much due to the stratification (particularly at greater heights).*
  - Changed this sentence to reflect this fact.
- *p19 table 2: Maybe better to also express this as percentage instead of number of obs.*
  - Adapted the table.
- *p19l7: It is not clear to me how the lidar measurements are normalized: with the friction velocity from the OBS run?*
  - Clarified formulation. Simulated friction velocity and heat flux is used to categorize and normalize LiDAR data.
- *p26: Remove Appendix A, it is not discussed anywhere.*
  - removed figures in appendix A1.

III. Technical corrections

- *p5l20: "(see equation: 2)" –> "(see Eq. 2)"*
- *p9 Fig 4 label: Abbreviation HWS is not defined*
- *p14l2: 100m –> 100 m (and m not in italics).*
- *p17l2: to (Sommerfeld et al.) –> to Sommerfeld et al. Also I don't know the journal policy but usually you can only include references that are 'accepted' and not those that are 'in review'.*
- *p17l4: ? –> ref*
- *p20l3-4: These two lines repeat the same thing.*
- *p20l5: ?? –> ref*
- *p21l7: Please split equation and units.*
- *p21l10: drag coefficient and drag coefficient? Also equal sign is not enclosed in '$'.*
- *p22 Fig. 13 caption: there is mention of a),b),c) here but they are not in the figure.*
- *p23l14: decreases –> decreases.*

- All technical corrections above have been addressed.

Markus Sommerfeld
Institute for Integrated Energy Systems
University of Victoria
3800 Finnerty Rd
Victoria, BC, Canada
V8P 5C2

June 28, 2019

Revision to wes-2019-7: Improving mesoscale wind speed forecasts using LiDAR-based observation nudging for Airborne Wind Energy Systems

Dear Prof. Schmehl,

Thank you very much for your helpful review of our manuscript, "Improving mid-altitude mesoscale wind speed forecasts using LiDAR-based observation nudging for Airborne Wind Energy Systems", wes-2019-7. We have modified the manuscript accordingly, removed or consolidated several figures and adapted the text.

Please find our response to individual comments below.

Changes are highlighted in the "Supplementary Material" pdf. Text and figures marked in red were removed from the original submission and replaced by text and figures marked in blue. Following are our replies to your comments and a description of modification to the manuscript.

Sincerely,
Markus Sommerfeld

Comments by the Referee

I. General comments

This paper about an airborne wind energy resource assessment is a valuable contribution. The focus is clearly on the improvement of the wind speed forecast at higher altitudes using LiDAR data. A relatively small part is about the use of this wind data for the prediction of power production from AWES.

The description of the simplified power production model in Section 4.7 is unclear and inhomogeneous. On the one hand, very specific derivation steps of the original derivation are mentioned (geometric relation of aerodynamic force components and apparent wind velocity components) that are not of interest within the scope of this paper and would require proper illustrations and more background information. Other aspects that would be important are however not discussed, for example assumptions and specific choices. I recommend to carefully revise this part of the paper.

- The sentence: "Additional losses caused by gravity, tether sagging and tether drag are neglected" summarizes some of the assumptions
- steady state assumption, constant c_L and c_D are mentioned in the text
- added tether sagging and point-mass assumption
- removed equations and simplified the derivation.

The original model of Schmehl et al (2013), that was also used as a basis for many other studies, is independent of tether length, as it is also apparent from your Equation (5). What was then the reason for you to choose a constant tether length of 1500 m? And how does the tether length come into play? This should be clearly described.

- Agreed.
- The equation is a function of elevation angle. The optimal elevation angle is calculated from the constant tether length and operating altitude.
- Added additional sentences:
  - Optimal elevation angle (ε_{opt}) and operating altitude (z_{opt}) are geometrically related to the assumed to be constant tether length (L_{tether}) of 1500 m ($\sin \varepsilon_{opt} = \frac{z_{opt}}{L_{tether}}$).
  - The tether length of each estimation is assumed to be constant and used to calculate the optimal elevation angle.
- Do you think the equation $\sin \varepsilon = \frac{altitude}{L}$ is necessary?

If you would account for tether drag, the performance of the AWES would decrease with increasing tether length (compared to the idealized case of no tether drag). Tether drag could, for example, be taken into account by an additional drag contribution and lumping this to the kite, as some authors do. A possible reference could be van der Vlugt (2019). But I assume that this was not done in the paper, for the purpose of simplicity? If so, please state this, as it is important when considering large ranges of tether length. For a implemented real AWES it makes generally sense to fly on a shorter tether when flying at lower altitudes, to reduce the effect of tether drag.

- Yes this is out of scope for this paper.
- The following sentences already address the additional losses associated with a longer tether:
  - All estimates show diminishing benefits of a longer tether. These incremental gains would probably be negated by additional drag and weight associated losses.

For a pumping AWES, which is considered here, the tether length continuously varies. Assuming a constant tether length is seemingly in contradiction with this and should thus be motivated better. Just "Here we assume a constant tether length" is not sufficient in my opinion. I would also like to know, if the choice of the constant tether length could possibly influence the results displayed in Fig. 13 (for this is must be clarified how tether length actually enters the modeling).

- See previous comments above

II. Specific comments

1. Authors

- *I believe that the Fraunhofer IWES location at Bremerhaven, Germany, is meant, and not Oldenburg?*
  - While the headquarter of Fraunhofer IWES is in Bremerhaven, IWES has several other locations in Oldenburg, Bremen, Hannover, Bochum and Hamburg. Gerald Steinfeld and Martin Dörenkämper work from Oldenburg.

2. Abstract

- *I would spell out WRF once, as you do with AWES.*
  - A definition of WRF was added to the abstract.

3. Introduction

- *Add a reference to Bechtle et al (2019). This could for example be done on p. 2, l. 14, just after Archer and Caldeira (2009).*

– Reference added.

- *Uwe Fechner (2016) describes in his dissertation and a later book chapter a turbulence model for AWES, based on the Mann turbulence model. As you shortly mention conventional spectral wind models (Burton, 2011) this might be worth a discussion point. (https://doi.org/10.1007/978-981-10-1947-0_15)*

  – Reference added.

- *p. 2, l. 23: You state "No mid-altitude measurement device can reliably gather long term, high frequency data." but do not give any reason for this. This statement should also be better embedded in the surrounding text.*

  – Added a sentence and references

- *p. 2, l. 25: Your reference to future work (complementation of TI estimates with LES data) is better for the conclusions section.*

  – Sentence removed and added to conclusion section.

- *p. 2, l. 28: Add a reference to the Onkites II project report, available from https://doi.org/10.2314/GBV:1009915452 Can the measurement data of OnKites II be made publicly available, as a data reference to complement this and the earlier paper? This would increase the value of this research tremendously (reproducibility!).*

  – Reference added. I can not make the decision to publish the data myself and have to refer you to Adrian Gambier and Julia Gottschall.

4. Mesoscale Modeling Framework

- *p. 4, l. 16: For the non-experts of this specific technique it would make sense to elaborate on the "non-physical forcing term". Why non-physical? Why not physical?*

  – The additional term is added to the conservation equations that guide the simulation. It is non-physical in nature since it is not based on any physical principle in contrast to the conservation of mass and momentum for example from which the conservation equations are derived. This additional term which is driven by the difference between measurement and simulation nudges the simulation closer to measurement without creating discontinuities in the simulation.

  – Added a subordinate clause: "...non-physical forcing term which is added to the governing conservation equations of the simulation to gradually nudge..."

- *p. 4, l. 18: It is unclear what the use of 3 nested domains is. Please clarify. What is η-pressure? (also "η-levels" in l. 23)*

  – The sentence explains the benefit of nested domains which is that the inner domains have higher spatial and temporal resolution.

  - added: ... along the terrain following vertical hybrid pressure coordinate η.

- *p. 4, l. 25: Again for the non-experts: what is the difference between "observation nudging" and "analysis nudging"? Maybe a pointer to the respective subsections, where you explain this, is sufficient.*
  - Added an additional sentence explaining the difference between analysis and observation nudging:
    * For analysis nudging each grid point is nudged towards a time-interpolated value from gridded analyses of synoptic observations whereas observation nudging directly drives the simulation towards observations.
  - Reference: In analysis nudging, the model fields are nudged at every grid point toward an analysis of the observations on the model grid in a manner such that the nudging term is proportional to the difference between the model and the analysis at each grid point (ref: `https://pdfs.semanticscholar.org/1c94/a18e5ce2edd5fa5189dc293d8d33fe46b7c7.pdf`)

- *p. 5, l. 4: What is the meaning of "qm interpolated"? And what means "(q0)"?*
  - This sentence explains equation 1 which defines the additional forcing term introduces by observation. This forcing term is driven by the difference between observation q_o and model q_m
  - q_m is the modeled quantity (e.g. wind velocity component, temperature, humidity etc...) which has to interpolated to the location of the additional observation due to the large grid size of mesoscale simulations
  - q_o is the observed quantity
  - No changes to the manuscript

- *p. 5, l. 9: "hydrostatic"? This paper is about atmospheric flows.*
  - Correct. This is part of the model.

- *p. 5, l. 13: The time expression in the bracket is not correctly written. It is not the mathematical constant 2.71828 that is meant here, because this would lead to 9 seconds.*
  - replaced by: $1/6\ 10^{-4}s$

5. Results

- *Elaborate on how unavailability of LiDAR data is handled for the nudged simulations.*
  - Added sentence in subsection 'Observation Nudging': Nudging could not be performed at times and altitudes where LiDAR data was not available.

- *p. 8, l. 3: RSME is missing in legend.*

  - added RMSE to the legend

- *p. 8, l. 5: The reduction of the spread of the bias is hard to observe by eye*
  - The reduction in bias spread (visualized by the lengths of the horizontal blue and red lines, also called whiskers) is clearly visible in the PDF.

- *p. 8, l. 9: Doesn't nudging reduce the error? So, reduced nudging would result in larger error?*
  - Good point. Subordinate clause removed.

- *p. 9, l. 14: Please elaborate on this sentence.*
  - Need more information. page 9 is referenced n this and the following comments. Probably page 8
  - added: ... as can be seen in the right box plot in figure 3

- *p. 9, l. 11: Bechtle et al (2019) have used a similar representation as the one described here, using dots to show the optimal altitude for operation of an AWES. A reference should thus be added, and possibly also a discussion of the usefulness of this measure added (i.e. an AWES will generally sweep an altitude range, which means that this single point characterization is only a very rough measure.)*
  - While we agree that a discussion is useful, we disagree that the usage of dots to visualize optimal altitude justifies the added reference. The same reference as been cited earlier in the paper.
  - Added sentence: A single point is only a rough measure of operational altitude since AWES generally sweep a range of altitudes.

- *p. 9, l. 14: How do you see that the LLJ and the .... are weaker? I can hardly see anything.*
  - The color of the contour plot in the upper subplot, which is refers to the horizontal wind speed, is significantly different between OBS and NoOBS.

- *p. 11, l. 7: You write "remain the same". Shouldn't ΔV be zero?*
  - That is right. While the boundary condition ($\Delta U = 0$) is applied on the outward facing surface of the cubic grid cell the wind speed values are stored and interpolated to the center of the grid cell. This leads to $\Delta U \neq 0$ at the boundary grid cell.
  - Added sentence: $\Delta U \neq 0$ because wind speed values are interpolated to the center of each grid cell.

- *p. 11, l. 8: You write "change in wind speed": is this observed by the gradient?*
  - can be seen by the spike of the red line close to the vertical black line.
  - Added subordinate sentence: ... measurement location which is highlighted by the black vertical line ...

- *p. 14-15, Figs. 7 and 8: Why are contour plots of Fig. 7 not as smooth as respective plots of Fig. 8. The caption mentions "filtered": aren't these "unfiltered"?*
  - As mentioned in the text: these contour plots are filtered by LiDAR availability. As a results, WRF data is discarded at times when LiDAR is not available. Therefore, the WRF results are skewed, but similar to LiDAR measurements.

- *p. 20, l. 3: You write "We chose": how do you control this?*
  - This has been addressed together with comments from the second Referee.

- *p. 21, l. 8: "Misalignment" is between TETHER and wind direction. It should be clear that the azimuth and elevation angles describe the angular position of the kite or aircraft with respect to the ground station. Renaming of Θ as elevation angle is dangerous, because it is generally use for the polar angle.*
  - Changed elevation angle to ε
  - Changed sentence to: Losses associated with mispositioning of the aircraft relative to the wind direction, expressed by azimuth angle ϕ, elevation angle ε relative to the ground station, are included in the model.

6. Conclusions

- *I am missing some conclusions of Section 4.7 on the AWES power estimation.*
  - reworked conclusion paragraph on AWES.

III. Language and style comments

1. General spelling

- *Use of dashes should be checked (e.g. "high-resolution data" or "long-term statistics" would be correct)*
  - hyphen added to the best of my knowledge

- *Do not capitalize abbreviations*
  (see https://www.aje.com/en/arc/editing-tipcapitalization-when-defining-abbreviations/).
  - removed capitalization in abbreviations except for names.

2. Title

- *p.1: "Airborne Wind Energy" should be "Airborne wind energy".*
  - removed capitalization, changed to “airborne wind energy”

3. Abstract

- *p. 1, l. 9: I would add an "it" between "but" and "becomes"*
  - pronoun “it” is omitted since there is no ambiguity that the topic of the sentence is the impact of nudging.

4. Introduction

- *p. 2, l. 4: "Airborne Wind Energy Systems" should be "Airborne wind energy systems".*
  - fixed capitalization
- *p. 2, l. 4: I would say that AWES are a class of renewable energy technologies, and not a source of energy. The source is the wind.*
  - Implemented.
- *p. 2, l. 10: Instead of "marketplace" I would just write "market".*
  - Implemented.
- *p. 2, l. 11: ...none are YET commercially available.*
  - changed to: ...none are currently commercially available
- *p. 2, l. 13: "power" should be "power output" as you list wind energy technologies here.*
  - Implemented.
- *p. 2, l. 23: ... variations to resolved quantities are parametrized. The "resolved" sounds wrong and the meaning of this sentence is also not clear to me.*
  - Corrected the sentence: Sub-gridscale high frequency variations **of** resolved quantities are parameterized.
- *p. 2, l. 25: "here presented" -> "presented in this study"*
  - Sentence removed in process of editing the manuscript.
- *p. 2, l. 27: Year is missing in reference.*
  - Reference updated
- *p. 3, l. 1: "power" -> "power output".*
  - Implemented.

5. Measurement campaign

- *p. 4, l. 2: Year is missing in reference.*
  - Reference updated
- *p. 4, l. 3: Should be "emphasizes".*
  - Implemented.
- *p. 4, l. 6: Should be "... the WRF-calculated...". The entire expression "WRFcalculated sensible surface heat flux (SHF)" sounds incomprehensible to me. What is the role of the "sensible"?*
  - Added hyphen.
  - Latent and sensible heat are types of energy released or absorbed in the atmosphere.
    - "In meteorology, latent heat flux is the flux of heat from the Earth's surface to the atmosphere that is associated with evaporation or transpiration of water at the surface and subsequent condensation of water vapor in the troposphere." `https://en.wikipedia.org/wiki/Latent_heat`
    - "In meteorology, the term 'sensible heat flux' means the conductive heat flux from the Earth's surface to the atmosphere." `https://en.wikipedia.org/wiki/Sensible_heat`
- *p. 4, l. 9: Should be "... the SHF".*
  - Implemented.
- *I would move Fig. 1 to the next section and remove the reference to the white X here. Because in the next section you explain the 3 hierarchically nested domains used for the WRF. Here, in this section, the figure introduces more questions than answers.*
  - Figure was moved to section 2.
  - Reference to white X was kept to show the measurement location and the location where observations were implementation.

6. Mesoscale modeling Framework

- *p. 4, l. 14: Year is missing in reference. It is also not clear whether the "section 2" in the referenced paper or the present one is meant.*
  - Citation updated and section 2 removed.
- *p. 4, l. 15: Year is missing in reference.*
  - Citation updated.

- *p. 4, l. 17: Why discussing here spatial resolutions when this is all given in Table 1?*
  - Spatial resolution is kept in the sentence and table removed.
- *p. 4, l. 23: "Turbulent Kinetic Energy" should be "Turbulent kinetic energy". Add "(TKE)" here and use the abbreviation in the next sentence.*
  - Replaced by "turbulent kinetic energy".
- *p. 4, l. 29: Maybe a footnote link with the URL is better? This bibliographic reference looks strange.*
  - Removed citation and replaced with footnote: "EDDY: HPC cluster at the Carl von Ossietzky Universität Oldenburg, see: `https://www.uni-oldenburg.de/fk5/wr/hochleistungsrechnen/hpc-facilities/eddy/`"
- *p. 5, l. 20: Something is wrong after W_{xy}.*
  - Fixed equation variable

7. Results

- *p. 6, l. 5: Should be "differences".*
  - Implemented.
- *p. 7, Fig. 2, legends: text and number should be separated by a space and also a comma.*
  - Updated legend to: linear regression, slope: 0.985.
- *p. 9, l. 2: Replace "bias" by "error".*
  - Implemented.
- *p. 17, l. 3: Reference missing (?).*
  - Citation updated.
- *p. 19, Table 2: last three columns in % of time would be better readable.*
  - Implemented.
- *p. 20, l. 4: "additional two" -> "two additional"*
  - Paragraph updated while editing.
- *p. 20, l. 5: Figure reference is missing (??).*
  - Paragraph updated while editing.
- *p. 21, l. 6: Why do you use a subscript "air" for the density? This study is only about atmospheric flows, so the index can be safely omitted.*

– That is correct. However, we chose to keep the subscript “air” for clarity.

- *p. 21, l. 7: Set equation in displaymode.*
  – kept equation in text. Could be changed when typesetting the manuscript.
- *p. 21, l. 10: "... are assumed constant are ...": something is wrong here*
  – Changed sentence to: “ ... and drag coefficient (c_D =0.06), which are assumed to be constant, are geometrically related to ...”

8. Conclusions

- *p. 23, l. 7: Six months OF LiDAR .....*
  – Implemented.
- *p. 23, l. 13: Dot behind "decreases" is missing.*
  – Paragraph changed while editing the manuscript.

9. Appendices

- *p. 25, Figure A1: what means the question mark at the end of this caption? "U profile" -> "velocity profile".*
  – Removed figure.
- *p. 25-26, Table A1: Include in the caption to which software & version, possibly also model, these settings refer.*
  – Caption updated to: “Namelist parameters for WRF 3.6.1 observation nudging”

10. References

There are many references for which the DOI is occurring twice, as "doi:..." and as URL "https://doi.org/...".
removed URL and kept DOI where applicable.

- *p. 28, l. 13: what is this oCLC number? I would use either ISBN or DOI.*
  – removed oCLC and replaced with DOI.
- *p. 28, l. 19: Publisher or standard-issuing organization is missing.*
  – updated reference to ISO 2533:1975
- *p. 29, l. 15: Correct the URL.*
  – Citation replaced with footnote.
- *p. 29, l. 23: Add DOI.*

  - Citation correct, long, long list of contributers followed by a DOI and URL

- *p. 29, l. 27: Insert comma/dot and space between "2016" and "At".*
  - Not sure where. No 2016 in this citation.

- *p. 30, l. 3: "Statistik" should be starting with a capital "S", according to German spelling. Consider choosing an English textbook as reference.*
  - Replaced reference.

- *p. 30, l. 8: This is a contributed chapter in a book. Accordingly the reference should be Schmehl, R., Noom, M., van der Vlugt, R.: Traction Power Generation with Tethered Wings. In: Ahrens, U., Diehl, M., Schmehl, R. (eds.) Airborne Wind Energy. Springer, Berlin Heidelberg, 2013.*
  - The citation is taken directly from: `https://link.springer.com/chapter/10.1007/978-3-642-39965-7_2` . Had to change @inbook to @incollection to make it work.

- *p. 30, l. 14: Update this*
  - Updated.

Markus Sommerfeld
Institute for Integrated Energy Systems
University of Victoria
3800 Finnerty Rd
Victoria, BC, Canada
V8P 5C2

June 30, 2019

Revision to wes-2019-7: Improving mid-altitude mesoscale wind speed forecasts using LiDAR-based observation nudging for Airborne Wind Energy Systems

Dear Dr. Bechtle,

Thank you very much for your helpful comments to our manuscript, "Improving mesoscale wind speed forecasts using LiDAR-based observation nudging for Airborne Wind Energy Systems", wes-2019-7. We have clarified the definition of RMSE and added additional reference to technical document describing the LiDAR uncertainty.
Following are our replies to your comments and a description of modification to the manuscript.

Changes are highlighted in the "Supplementary Material" pdf. Text and figures marked in red were removed from the original submission and replaced by text and figures marked in blue. Following are our replies to your comments and a description of modification to the manuscript.

Sincerely,
Markus Sommerfeld

Comments by the Referee

I. General comments

Dear Authors, congratulations for your very interesting and important analysis. I read the paper with great interest. I have one or two questions about the methods which lead to Fig. 3.

First, I am unsure about what you mean by "The continuous line in the left sub-figure represents the Root Mean Square Error (RMSE) of wind speed." This is just a question for clarification... The RMS of what? is it a measure of the temporal variation of the measured or simulated wind speed on its own within some interval? Or an estimate of the precision of simulation or measurement (and if that, how is that uncertainty derived?)? Or an RMS of a difference between different quantities? I think the paper would profit if you could explain this in more detail.

- A clearer definition of wind speed RMSE, which quantifies the error between LiDAR measurements and WRF simulations, has been added to the paper.

The other question, which maybe is connected to the first question, is about the uncertainty. Your measurement itself is subject to an uncertainty, and it would be interesting if that would be clearly described.

Thank you very much! Philip Bechtle

- We have added a reference to a technical report verifying the performance of the used LiDAR (`https://www.woodgroup.com/__data/assets/pdf_file/0023/15692/report_Sgurr_20130529_FINAL1.pdf`). Further information can be found in our previous paper "LiDAR-based characterization of mid-altitude wind conditions for airborne wind energy systems" (`https://doi.org/10.1002/we.2343`).

Markus Sommerfeld
Institute for Integrated Energy Systems
University of Victoria
3800 Finnerty Rd
Victoria, BC, Canada
V8P 5C2

June 30, 2019

Revision to wes-2019-7: Improving mid-altitude mesoscale wind speed forecasts using LiDAR-based observation nudging for Airborne Wind Energy Systems

Dear Dr. Saraceno,

Thank you very much for your comments on our manuscript, "Improving mesoscale wind speed forecasts using LiDAR-based observation nudging for Airborne Wind Energy Systems", wes-2019-7.
Our analyses focus on wind conditions up to 1100 m and apply a simplified ground-gen AWES model to estimate maximum power output and optimal altitude for this maximum power (neglecting tether weight and drag). These findings are representative for a specific location and time period in Northern-Germany, based on mesoscale wind and weather simulations and backed by a published study on LiDAR measurements at this specific location("LiDAR based characterization of mid altitude wind conditions for airborne wind energy systems" (`https://doi.org/10.1002/we.2343`).
Comparing different AWES designs and concepts is beyond the scope of this paper. We do not state that designing a system for maximum power and neglecting capacity factor is desirable. On the contrary, we hope that our findings, which are to our knowledge the best representation of actual wind conditions at higher altitudes, will educate designers, manufacturers and researchers to design more efficient and reliable systems.
Sincerely,
Markus Sommerfeld

Improving ~~mid-altitude~~ mesoscale wind speed forecasts using LiDAR-based observation nudging for airborne wind energy systems

Markus Sommerfeld[1], Curran Crawford[1], Gerald Steinfeld[2], and Martin Dörenkämper[3]

[1]Institute for Integrated Energy Systems, University of Victoria,British Columbia, Canada
[2]Institute of Physics-Energy Meteorology, Carl von Ossietzky Universität Oldenburg, Germany
[3]Fraunhofer Institute for Wind Energy Systems, Oldenburg, Germany

Correspondence to: Markus Sommerfeld (msommerf@uvic.ca)

Abstract.

Airborne wind energy system (AWES) aim to operate at altitudes above conventional wind turbines where reliable high-resolution wind data is scarce. Wind light detection and ranging (LiDAR) measurements and mesoscale models both have their advantages and disadvantages when assessing the wind resource at such heights. This ~~article~~ study investigates whether assimilating measurements into the mesoscale weather research and forecasting (WRF) model using observation nudging generates a more accurate, complete data set. The impact of continuous observation nudging at multiple altitudes on simulated wind conditions is compared to an unnudged reference run and to the LiDAR measurements themselves. We compare the impact on wind speed and direction for individual days, average diurnal variability and long-term statistics. Finally, wind speed data is used to estimate optimal traction power and operating altitudes of AWES. ~~Observation nudging improves the overall accuracy of WRF.~~ Observation nudging improves the WRF accuracy at the measurement location. Close to the surface the impact of nudging is limited as effects of the air-surface interaction dominate, but becomes more prominent at mid-altitudes and decreases towards high-altitudes. The wind speed probability distribution shows a multi-modality caused by changing atmospheric stability conditions. Therefore, wind conditions under various stability conditions are investigated. Based on a simplified AWES model the most probable optimal altitude ~~will be around 400 m~~ is between 200 and 600 m. This wide range of heights emphasizes the benefit of such systems ~~will benefit from~~ to dynamically adjust~~ing~~ their operating altitude.

Keywords: Airborne Wind Energy, Wind Measurement, Onshore Wind, Weather Research and Forecasting Model, Observation Nudging, Statistic Wind Conditions, LiDAR, WRF

1 Introduction

The prospects of higher energy potential and more consistent strong winds and less turbulence in comparison to near surface winds sparked the interest in mid-altitude, here defined as heights above 100 m and below 1500 m, wind energy systems. airborne wind energy system (AWES) are a novel ~~renewable energy source~~ class of renewable energy technology that harvest stronger winds at altitudes which are unreachable by current wind turbines, at potentially much reduced capital cost (Lunney et al., 2017; Fagiano and Milanese, 2012). For practical and economical reasons we focus on resource assessment within the lower part of the atmosphere, an altitude range spanned by the highly-variable boundary layer. Unlike conventional wind energy which has converged to a single concept with three blades and a conical tower, several different AWES designs are under investigation by numerous companies and research institutes worldwide (Cherubini et al., 2015). Various concepts from ring shaped aerostats, to rigid wings and soft kites with different sizes, rated power and altitude ranges compete for entry into the market~~place~~. Since this technology is still in an early stage, none are currently commercially available.

Developers and operators of large conventional wind turbines, AWES and drones require accurate wind data to estimate power output and mechanical loads. They currently rely on oversimplified approximations such as the logarithmic wind profile (Optis et al., 2016) or coarsely resolved reanalysis data sets (Archer and Caldeira, 2009; Bechtle et al., 2019) as the applicability of conventional spectral wind models (Burton, 2011) have not been verified for these altitudes. First investigations (Fechner and Schmehl, 2018) resorting to the Mann model (Mann, 1994; IEC, 2005) have been conducted.

Recent advancements in wind LiDAR technology enable ~~high-resolution~~ measurements ~~in~~ at higher altitudes. This measurement technique however suffers from reduced data availability with increasing altitude caused by a decrease in aerosol density which is needed for the backscattering of the LiDAR signal (Peña et al., 2015). No mid-altitude measurement device can reliably gather long-term, high-frequency data. Temporal and spatial resolution of LiDAR devices is insufficient to precisely measure high-frequency fluctuations, but estimated turbulence intensity correlates with sonic turbulence measurements for lower altitudes (Sathe et al., 2011). Balloon mounted sonic anemometer are in early development (Canut et al., 2016). The expensive and time consuming nature of ~~LiDAR~~ measurements motivates the usage of numerical weather prediction (NWP) models such as the mesoscale model weather research and forecasting (WRF) as an adequate tool to assess synoptic characteristics of the atmospheric boundary layer (ABL) (Al-Yahyai et al., 2010). These models typically have a spatial resolution that ranges from one kilometer to tens of kilometers and a temporal resolution in the order of minutes. Sub-gridscale high-frequency variations ~~to~~ of resolved quantities are parameterized. Mesoscale models can be used to produced long-term reference data sets up to higher altitudes such as the New European Wind Atlas(Witha et al., 2019) ~~No mid-altitude measurement device can reliably gather long-term, high-frequency data. However, LiDAR estimated TI correlate with sonic turbulence measurements for lower altitudes~~ (Sathe et al., 2011). ~~As such the here presented TI estimates only present a rough estimate and will be complemented with high-resolution large eddy simulations data presented in future work.~~

This work is a continuation of a previous investigation of mid-altitude wind LiDAR measurements (Sommerfeld et al., 2019). The measurements used in these studies were gathered as part of the *OnKites II* project (Gambier et al., 2017) at the Fraunhofer institute for wind energy systems (IWES) with the goal of evaluating the potential of AWES. This paper makes use of various

statistical tools to describe the relationship between the mesoscale WRF model and LiDAR measurements to determine the impact of wind speed observation nudging (Mylonas-Dirdiris et al., 2016).

Section 2 describes the measurement campaign. Section 3 introduces the mesoscale model and observation nudging methodology used in this article. Section 4 quantifies the impact of observation nudging and summarizes the statistical differences between WRF and LiDAR. Results are applied to estimate optimal operating altitude and power output based on a simplified AWES model in section 4.7. Section 5 concludes the article with an outlook and motivation for future work.

2 Measurement Campaign

The LiDAR data used in this study (Bastigkeit et al., 2017) were collected between September 1st, 2015 and February 29th, 2016 at the 'Pritzwalk Sommersberg' airport (Coordinates: Lat: 53° 10' 47.00"N, Lon: 12° 11' 20.98"E) in Northern Germany (see white X in figure 2). The area surrounding the airport mostly consists of flat agricultural land with the town of Pritzwalk to the South. A *Galion4000* single beam pulsed wind LiDAR from SgurrEnergy was used (Gottschall et al., 2009). Wind speed data were collected using the doppler beam swinging (DBS) method (opening angle of 62°) which averaged multiple line of sight measurements at constant elevation angle and four azimuth angles to calculate the 10 min mean wind speed at 40 range gates up to an altitude of about 1100 m. Reference measurement found the mean LiDAR error to be around 1% with a standard deviation of 5% (Gottschall, 2013). The resulting wind speed is inherently spatially and temporally averaged. At an altitude of 1100 m the radius of the averaging disc defined by the four azimuth positions with 90° increments is about 585 m. For the reconstruction of 10 min mean wind speed it is thus assumed that the wind vector does not change over this area, a valid assumption for these heights over flat terrain.

LiDAR data availability highly depends on the applied carrier-to-noise ratio (CNR) filter and the aerosol content of the air as the wind speed is calculated based on the backscatter of the emitted laser beam. Most aerosols originate from the surface and are transported aloft. Particle density decreases with height and drops to almost zero within the free atmosphere above the ABL (Matthias and Bösenberg, 2002). Data quality quantified by the CNR dropped on average by approximately 5 dB over the course of 1000 m. A fixed CNR threshold of $CNR_{dB} > -25$ dB combined with additional self-defined filters (Sommerfeld et al., 2019) were applied and insufficient data was discarded. As a result, data availability dropped from about 81% at 100 m and about 24% at 1000 m. Low data availability caused by weather effects (e.g. strong precipitation) further emphasizes the importance of simulations for mid-altitude wind resource assessment as no measurement technique with sufficient spatial and temporal resolution is available at this point.

~~Unstable and stable stratifications were identified by partitioning the data based on the sign of WRF-calculated sensible surface heat flux (SHF). These two atmospheric conditions lead to bi-modal wind speed probability distributions aloft which is not adequately represented by a single Weibull distribution fit. Mid-altitude wind speeds are better represented by the weighted sum of two wind speed probability density function (PDF) fits conditioned by the sign of the SHF.~~

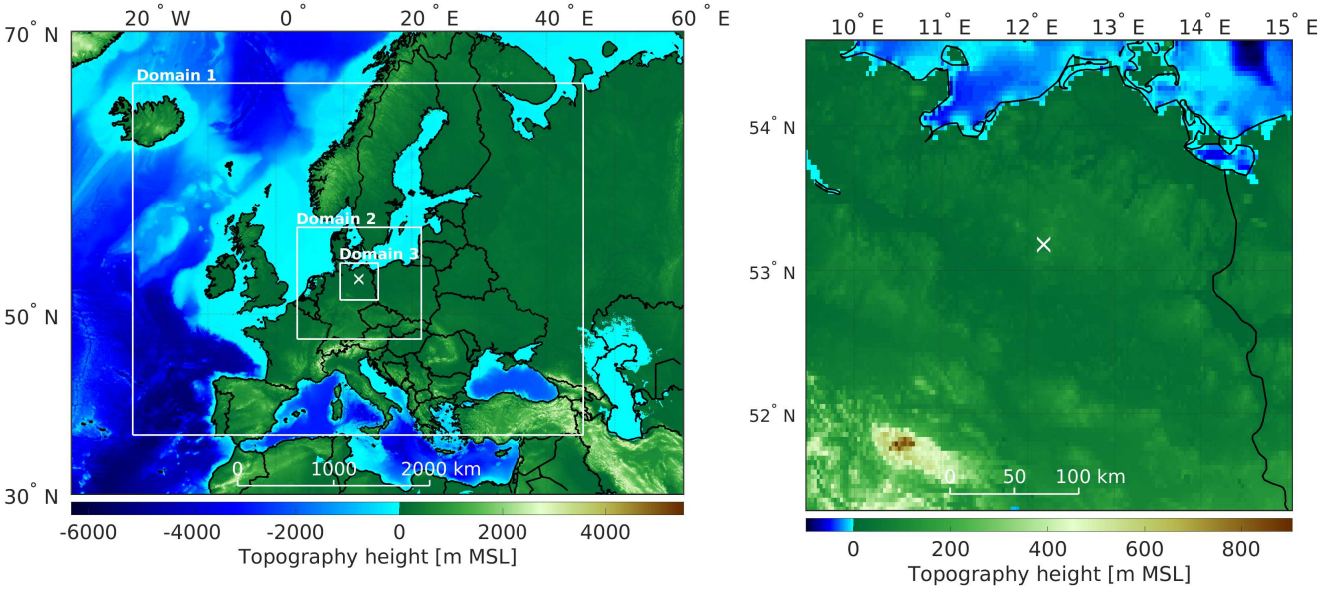

(a) Three nested WRF domains

(b) Inner WRF domain

Figure 1. ~~Topography map of all three WRF model domains (a) and a magnification of the innermost domain (b) with the LiDAR measurement site marked by a white X.~~

3 Mesoscale Modeling Framework

To complement the 6 months LiDAR data set two WRF ~~(v.~~ 3.6.1~~)~~ simulations using the advanced research weather research and forecasting (ARW) model (Skamarock and Klemp, 2008) were carried out. The 'baseline run' ~~(~~, which is hereinafter referred to as *NoOBS*, ~~)~~ is a 12 month study of the area around the measurement location (see figure 2) from the 1st of September 2015 used to derive annual statistics. LiDAR measurements (Sommerfeld et al., 2019) ~~(see section 2)~~ were incorporated into the six months test model between September 2015 and February 2016 using *OBSGRID* (Wang et al., 2015) ~~(~~, which is hereinafter referred to as *OBS*~~)~~.

This methodology uses the difference between model and measurements to calculate a non-physical forcing term ~~that~~ which is added to the governing conservation equations of the simulation to gradually nudge~~s~~ the model towards the observation (see equation 1) (Stauffer et al., 1991; Deng et al., 2007). Each simulation is composed of three nested domains with 27-, 9- and 3-km grid spacing and horizontal grid dimensions of about 120 $\times$ 120 elements at 60 ~~pressure~~ heights along the terrain following vertical hybrid pressure coordinate η. Differences between the simulation runs (see section 3.1) are compared within the innermost domain of the simulation. Output data was stored in 10 min intervals. Figure 2 shows the topography map of the simulation. Initial and boundary conditions of both simulations are based on the *ERA-Interim* (Dee et al., 2011) reanalysis data set by the European centre for medium-range weather forecasts (ECMWF) which consists of 6 hourly atmospheric fields with a spatial resolution of roughly 80 km horizontally and 60 η levels. Turbulent Kinetic Energy closure within the ABL was achieved

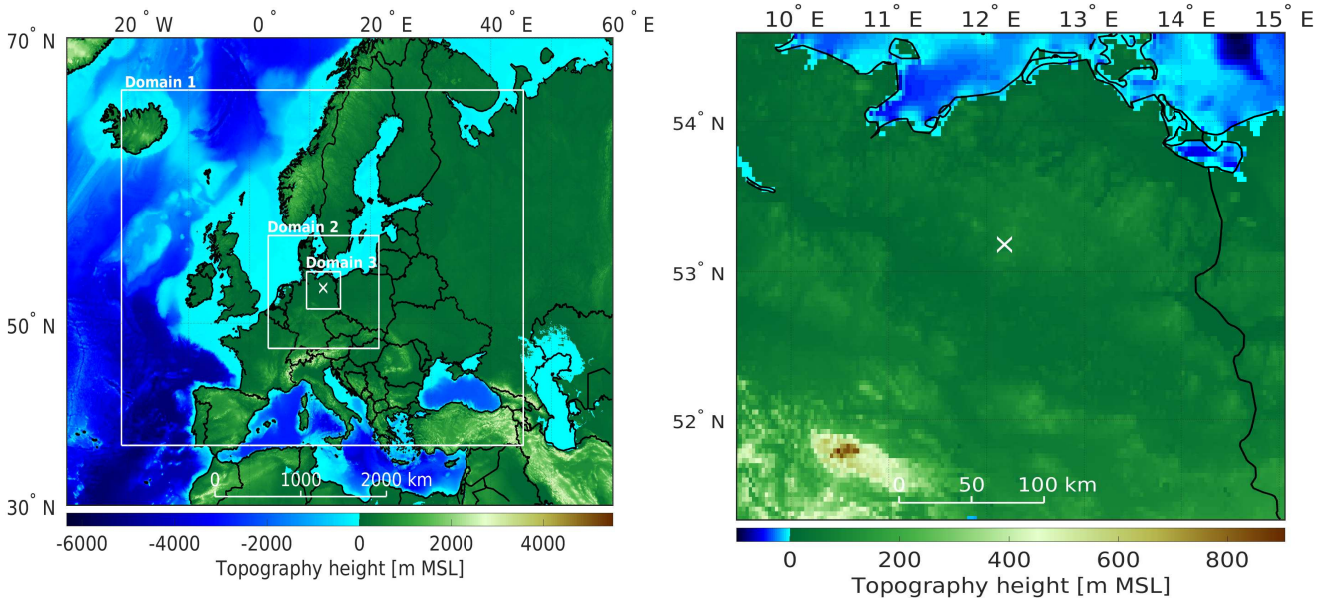

(a) Three nested WRF domains

(b) Inner WRF domain

Figure 2. Topography map of all three WRF model domains (a) and a magnification of the innermost domain (b) with the LiDAR measurement site marked by a white X.

by using the Mellor Yamada Nakanishi Niino (MYNN) 2.5 scheme which predicts sub-grid turbulent kinetic energy (TKE) as a prognostic variable (Nakanishi and Niino, 2004; Lee and Lundquist, 2017). The Noah-MP land-surface model, MYNN surface layer scheme were used. The rrtm long wave radiation and Dudhia short wave radiation scheme were used (see: table A1 in the appendix). In addition to observation nudging (see subsection 3.1) analysis nudging was performed on every domain of each simulation . ~~where~~ Analysis nudging nudges each grid point ~~is nudged~~ towards a time-interpolated value from gridded analyses of synoptic observations (Stauffer et al., 1991) whereas observation nudging directly drives the simulation towards the additional observations. Within the planetary boundary layer (PBL) of the inner domain analysis nudging was switched off (see nudging settings in table A1 in the appendix). All simulations were run on the *EDDY* ~~citation replaced with footnote~~ [1] High-Performance Computing clusters at the University of Oldenburg. ~~Table 1 summarizes the WRF domain size.~~

[1] EDDY: HPC cluster at the Carl von Ossietzky Universität Oldenburg, see: https://www.uni-oldenburg.de/fk5/wr/hochleistungsrechnen/hpc-facilities/eddy/

Table 1. ~~Resolution and grid size of WRF domains~~

Name	domain size [km x km]	grid spacing [km x km]	temporal resolution [sec]
Domain 1	3240x3240	27 x 27	90
Domain 2	1080x1080	9 x 9	30
Domain 3	360x360	3x 3	30

3.1 Observation Nudging

Observation nudging also referred to as 'dynamic analysis' is a form of four-dimensional data assimilation (FDDA) where each grid point within the radius of influence and time window is nudged towards observations using a weighted average of differences between model (q_m interpolated at the observation location) and observations (q_o) (Dudhia, 2012; Reen, 2016). In this study horizontal wind speed U and direction Φ were nudged towards measurements with a time interval of six hours between an altitude of 66 m and 1100 m, in order to not overly constrain the simulation. Nudging could not be performed at times and altitudes where LiDAR data was not available. The non-physical forcing term is implemented in form of prognostic equations (Deng et al., 2007):

$$\frac{\partial q\mu}{\partial t}(x,y,z,t) = F_q(x,y,z,t) + \mu G_q \frac{\sum_{i=1}^{N} W_q^2(i,x,y,z,t)\,[q_o(i) - q_m(x_i,y_i,z_i,t)]}{\sum_{i=1}^{N} W_q(i,x,y,z,t)} \tag{1}$$

q refers to the quantity that is nudged, μ is the dry hydrostatic pressure, F_q(x,y,z,t) is the physical tendency term of q, G_q is the nudging strength of q, N is the total number of assimilated observations, i is the index of the current observation, W_q is the weighting function based temporal and spatial separation between grid cell and observation (Dudhia, 2012). Four weighting functions G_q, $W_t(x,y,z,t)$, $W_z(x,y,z,t)$ and $W_{xy}(x,y,z,t)$ describe the temporal and spatial nudging strength. Values used in this study can be found in the appendix (table A1). The inverse of G_q (here about ~~$1/6e^{-4}s$~~ $1/6\ 10^{-4}s$ ≈ 46 min) can be interpreted as a nudging time scale as it dictates how quickly the model approaches the observation.

W_{xy} and W_z define the spatial nudging weight while the temporal weighting function W_t defines the duration and weighting strength in time. W_t ramps from 0 to 1 and back to 0 (Reen, 2016). The nudging time window and the time between implemented observations was chosen to be 6 hours so that the implemented observations don't overlap each other. This ensures all time steps are nudged while not excessively limiting the model.

Vertical influence was set very small so that observations only affect their own η level (Dudhia, 2012). The horizontal weighting factor W_{xy} (see equation: 2 is calculated based on the radius of influence R and the distance between the observation

and the grid location D. We used the 'Cressman scheme' as the horizontal nudging weighting function with a radius of influence of $R = 180$ km, thereby ~~containing~~ affecting the whole inner domain.

$$w_{xy} = \begin{cases} \frac{R^2 - D^2}{R^2 + D^2} & 0 \leq D \leq R \\ 0 & else \end{cases} \tag{2}$$

4 Results

It is important to keep the differences in temporal and spatial resolution between LiDAR measurements and WRF simulation in mind. Furthermore, data availability highly influences the ability to nudge the simulation (see section 2) and compare wind speed statistics.

To quantify the local effect of observation nudging, we investigate the cell closest to the LiDAR measurement location and compare measured and modeled horizontal wind speeds U and direction. Additionally we investigate several sections at different locations and altitudes within the inner domain to quantify the spatial and temporal impact of single location observation nudging on the entire domain. Vector values of each WRF cell are calculated on the faces of each cell, linearly interpolated to the cell center and rotated from the grid projection to earth coordinate system.

4.1 Impact of nudging on wind statistics

Figure 3 shows the scatter plots of measured and simulated horizontal wind speed at various altitudes for times at which LiDAR data is available. The continuous line represents the linear regression of the data (regression coefficient is displayed in the legend) while the dotted line shows an ideal correlation. The color of the scatter points corresponds to the ~~occurrence probability~~ frequency of occurrence. Multiple wind speed clusters caused by stratification can be identified. While there is a trend towards higher wind speeds with increasing altitude, low wind speeds (<~~8~~ 6 m/s) still occur at high-altitudes. Both simulations overpredict horizontal wind speeds at low-altitudes which is a known problem of WRF and could be attributed to the model not resolving sub-grid scale roughness elements properly (e.g. modeling strongly simplified parameterization of forests and/or cities) or flaws in the planetary boundary layer model which lead to overly geostrophic winds over land (Mass and Ovens, 2011). Observation nudging improves the overall correlation with measurements at the measurement location as surface influence decays. Both models approach similar values at higher altitudes which could be caused by the lack of observations and therefore observation nudging due to reduced data availability or is indicative of WRF generally being better at modeling more geostrophic winds.

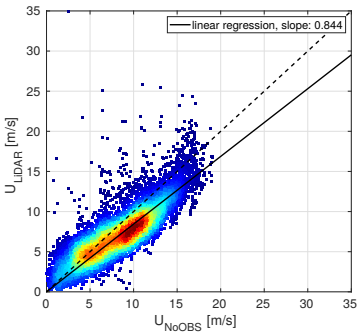

(a) LiDAR-NoOBS $z \approx 100$m

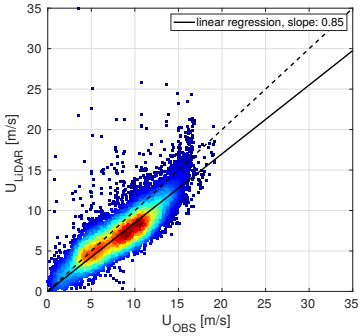

(b) LiDAR-OBS $z \approx 100$m

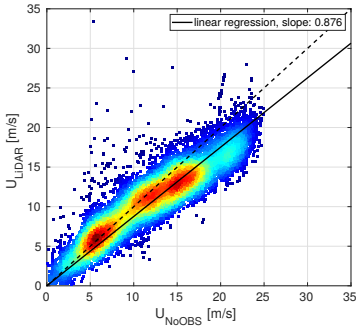

(c) LiDAR-NoOBS $z \approx 300$m

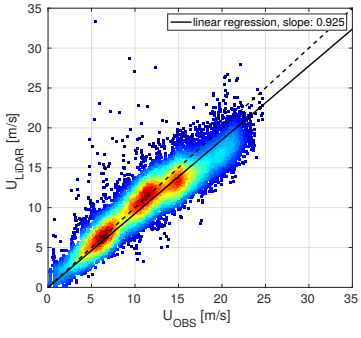

(d) LiDAR-OBS $z \approx 300$m

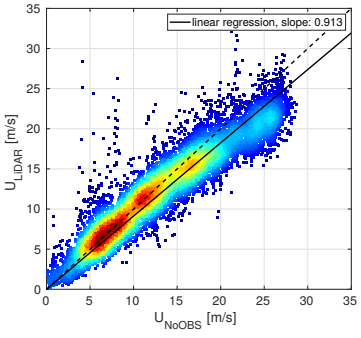

(e) LiDAR-NoOBS $z \approx 500$m

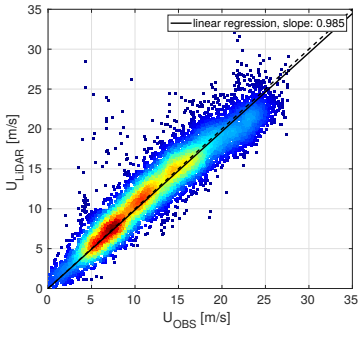

(f) LiDAR-OBS $z \approx 500$m

Figure 3. Linear Regression of LiDAR-measured wind speeds against NoOBS-modeled (WRF 'baseline run' without observation nudging) wind speeds (left side) and OBS-modeled ('test run' with obsgrid observation nudging) wind speeds (right side), at 100 m (a-b), 300 m (c-d), 500 m (e-f) **updated legend**

25 The statistical analysis of the absolute difference between the WRF simulated quantities at the measurement location and the LiDAR observations ($\Delta U = U_{WRF} - U_{LiDAR}$; $\Delta\Phi = \Phi_{WRF} - \Phi_{LiDAR}$ wrapped on an interval between $[-\pi, \pi]$) is shown in figure 4 in form of a box plot. The circle corresponds to the median, the colored box indicate the 25 % and 75 % percentile

and the whiskers to both sides mark ± 2.7 times standard deviation (σ). Outliers beyond $\pm 2.7\sigma$ are hidden to maintain clarity and readability. The continuous line in the left sub-figure represents the root mean square error (RMSE) ~~of wind speed~~ between the measured U_{LiDAR} and simulated wind speed U_{WRF}. ~~The unnudged simulation (NoOBS) shows an almost constant wind direction bias at all altitudes.~~

observation nudging (OBS) generally outperforms NoOBS and is in better agreement with the measurements particularly at altitudes of interest to high-altitude wind energy systems. It furthermore reduces the spread of the bias, illustrated by the smaller whiskers and boxes. The RMSE ΔU ~~of both simulations~~ shows similar results for both simulations below 100 m and above 700 m. The largest improvement or smallest error can be found between ~~250 m~~ 300 m and 600 m. This could be explained by a better performance of the mesoscale model at these altitudes due to a reduced impact of the air surface interaction ~~that~~ which is strongly parameterized ~~or due to a reduced nudging due to low LiDAR data availability~~.

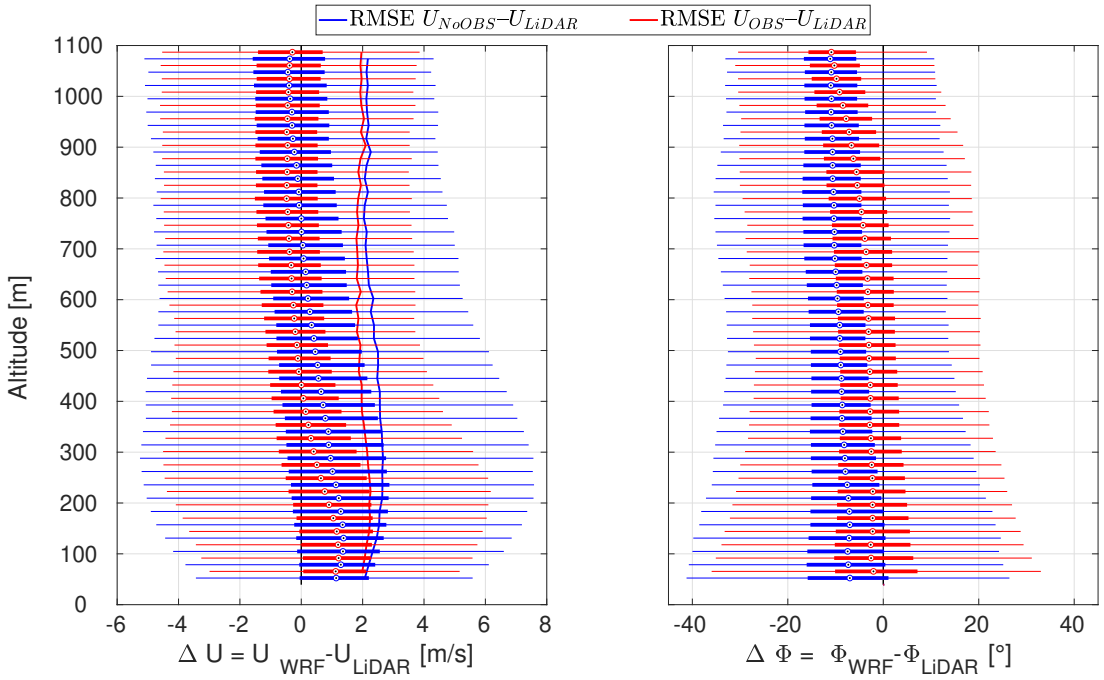

Figure 4. Statistical analysis of the bias between simulated and measured wind speed (ΔU) and direction bias ($\Delta\Phi$). The circle corresponds to the median, the colored box indicates the 25 % and 75 % percentile and the whiskers mark $\pm 2.7\sigma$. The solid lines in the left figure show the RMSE between the modeled and measured wind speed. **changed caption to include RMSE**

The NoOBS shows an almost constant wind direction bias at all altitudes. Observation nudging substantially reduces the directional bias $\Delta\Phi$ up to high-altitudes as can be seen in the right box plot in figure 4. Similar to the wind speed bias, wind direction bias at 1100 m is almost the same for both simulations. The negative wind direction bias represents an anti-clockwise deviation. Other studies (Carvalho et al., 2014; Giannakopoulou and Nhili, 2014) have found similar wind direction biases. A possible reason for this systematic ~~bias~~ error is that WRF does not adequately resolve surface roughness resulting in lower

surface friction leading to overly geostrophic winds (Mass and Ovens, 2010). The almost constant median wind direction bias indicates that WRF is able to capture the clockwise rotation of the 'Ekman Spiral' in the Northern hemisphere.

4.2 Representative nudging results

We compare 10 min mean horizontal wind speed for 24 hours on the 21st of September 2015 in figure 5 ~~(an additional day can be found in the appendix figure A1)~~ to visualize the impact of observation nudging on the mesoscale model output. White space in the LiDAR measurements (see figure 5a) are data points that have been filtered out due to insufficient data quality. The dashed line is the WRF modeled SHF used to estimate atmospheric stability (see sub-section 4.5). The color of the profiles indicate the wind direction and LiDAR measured profiles are shown in grey for comparison. The black dot in each profile marks the altitude of highest wind speed while the black circle indicates the optimal altitude for the operation of an airborne wind energy system based on a simplified power approximation (see section 4.7). However, the single point representation is only a rough measure of operational altitude since AWES generally sweep a range of altitudes.

Even though observation nudging leads to statistical improvements in wind speed and wind direction prediction over the entire period (compare sub-section 4.1 and 4.4), individual days can still show a decline in model accuracy. The low level jet (LLJ) as well as the high wind speeds at higher altitudes, which the NoOBS model captures fairly well, are significantly weaker in the OBS model. Implementing additional measurements at a higher frequency might yield results closer to measurements, but adding too many unphysical forcing terms might overly restrict the simulation.

The planetary boundary layer height (PBLH) (black line), which in the MYNN scheme is calculated from the profile of virtual potential temperature and from the profile of the TKE (Brunner et al., 2015; Nakanishi and Niino, 2004), is directly affected by wind speed observation nudging. During the investigated day, observation nudging leads to a lower daytime PBLH.

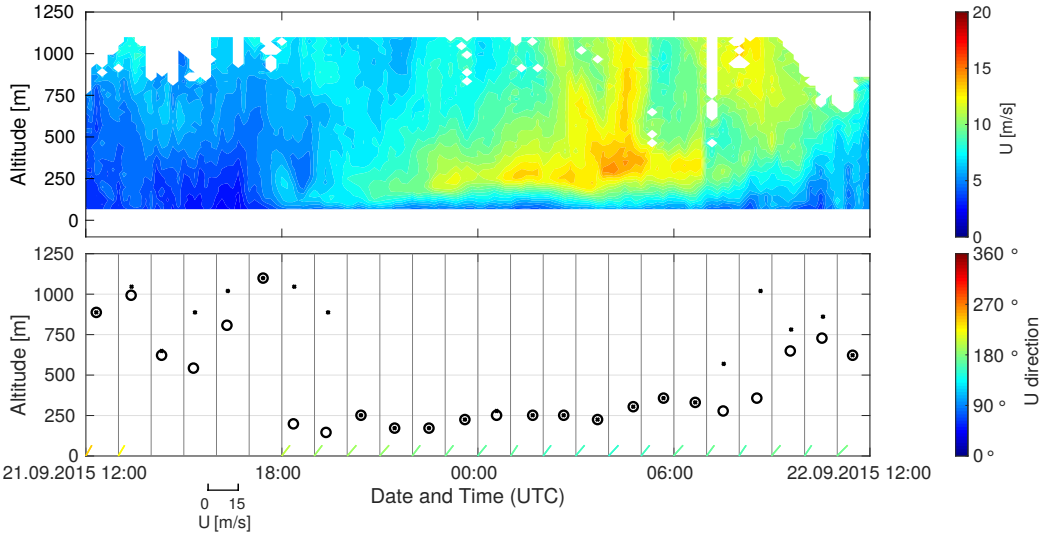

(a) LiDAR

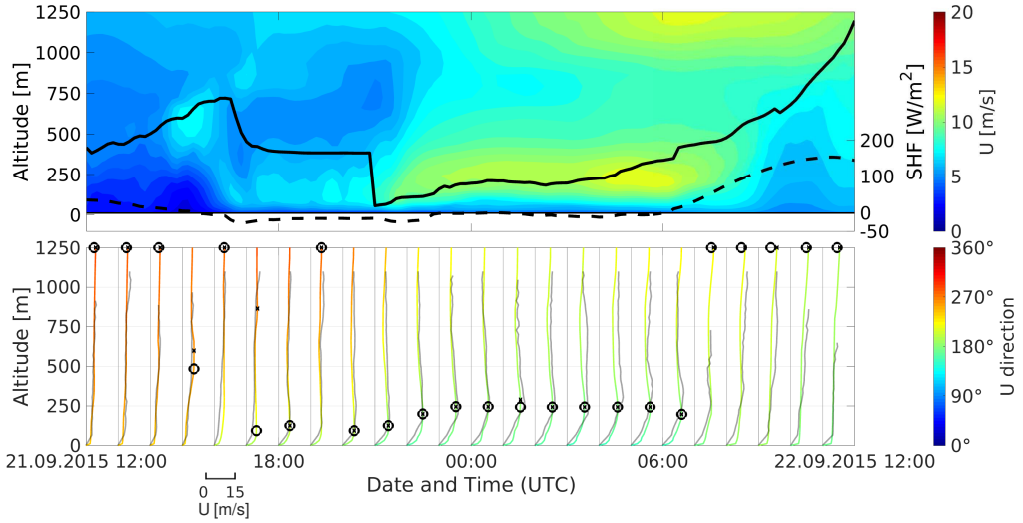

(b) OBS

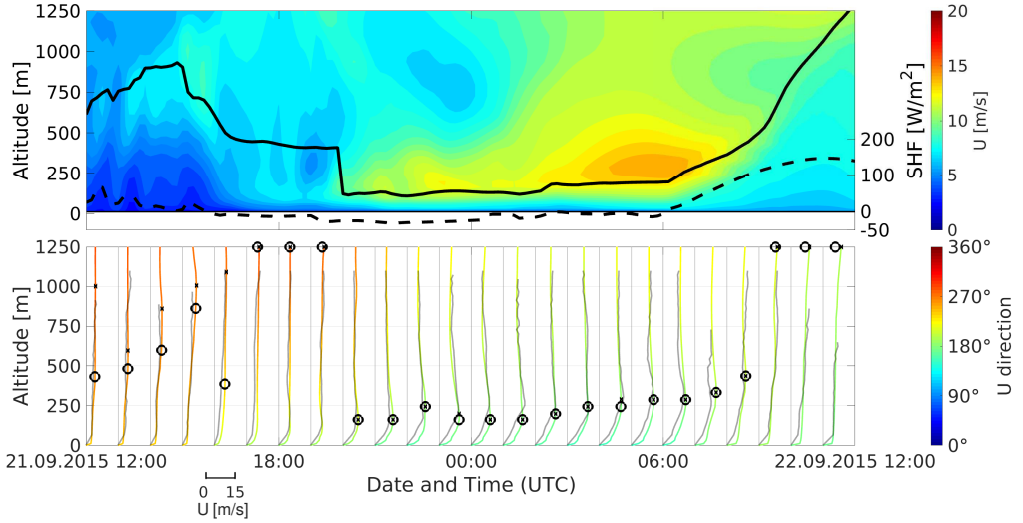

(c) NoOBS

Figure 5. Visualization of modeled and measured 10 min mean wind speed, wind direction for 21st September 2015. The respective top figure shows the wind speed and WRF calculated SHF (dashed line). The bottom figure shows each hours 10 min mean wind speed profile colored according to wind direction. X marks the altitude of highest wind speed and ◯ the optimal operating altitude calculated as described in section 4.7

4.3 Spatial influence

Single location observation nudging influences the area within the radius of influence ($R_{xy} = 180$ km, see table A1 in the appendix) which here includes the entire inner domain (150 km $\times$ 150 km). Figure 6 shows the mean absolute difference of horizontal wind speed ($\Delta U = |U_{OBS}| - |U_{NoOBS}|$) between the OBS and NoOBS model along lines of constant longitude and latitude for the entire simulation period. The grid cell where observations were assimilated is indicated by the vertical line and highlighted by the square marker. The four colors indicate different altitudes. As the outer domains remain unnudged, the boundary conditions of the inner domain remain the same which leads to the rapid decline in absolute difference towards the outside of the domain. The difference in wind speed $\Delta U \neq 0$ does not go to exact zero, because results are interpolated to the center of each grid cell. Near surface results close to the measurement location , which is highlighted by the black vertical line, experience the largest change in wind speed ~~especially close to the surface~~ (red line, z = 12 m). The asymmetry could be caused by the downstream transportation of nudging effects (dominant wind direction: West).

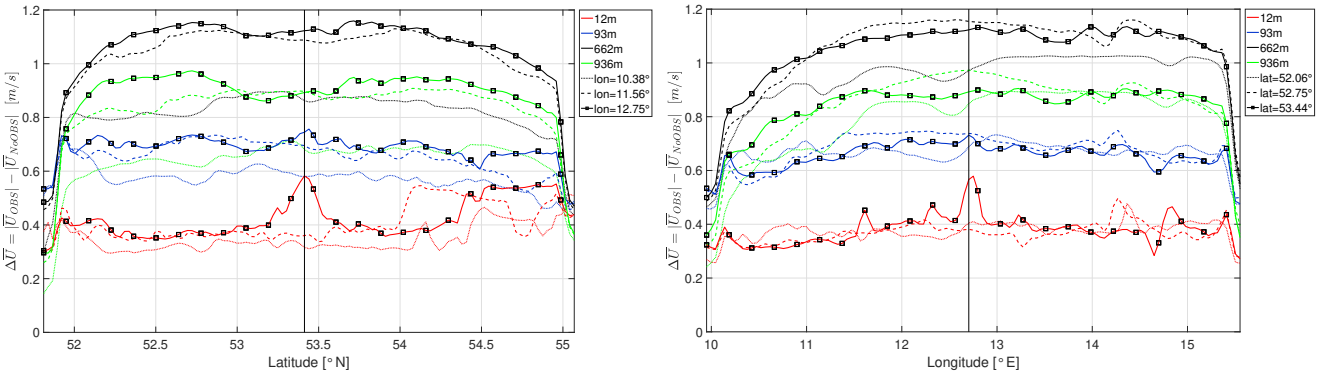

(a) ~~Mean absolute wind speed difference~~ $\Delta\overline{U}$ along lines of constant longitude. (b) ~~Mean absolute wind speed difference~~ $\Delta\overline{U}$ along lines of constant latitude.

Figure 6. Mean absolute wind speed difference $\Delta\overline{U}$ along lines of constant longitude (~~top~~ a) and latitude (~~bottom~~ b) within the nudged domain. Approximate distance of $d_3 \approx$ 180km (dotted lines), $d_2 \approx$ 75 km (dashed lines), $d_1 \approx 0$ km (solid line) from the center (Lat: 53° 10' 47.00"N, Lon: 12° 11' 20.98"E) Vertical line highlights the grid cell closest to observation.**reduced size of figures to fit next to each other**

~~The effect of observation nudging on horizontal wind speed remains almost unchanged along lines of constant longitude or latitude. The difference peaks between 400 m and 600 m and drops towards higher altitudes (as seen in figure 7) which shows the average absolute difference in wind speed along a slice of constant longitude and latitude through the center cell of the inner domain for the entire simulation period. Wind speeds at low and high altitudes are less affected by nudging while OBS wind speeds at mid-altitudes throughout the entire domain tend to be lower than the reference NoOBS. This can be attributed to surface and geostrophic effects dominating over observation nudging. The reduction in available high-altitude LiDAR data (see section 2) also reduces the effect of high-altitude nudging.~~

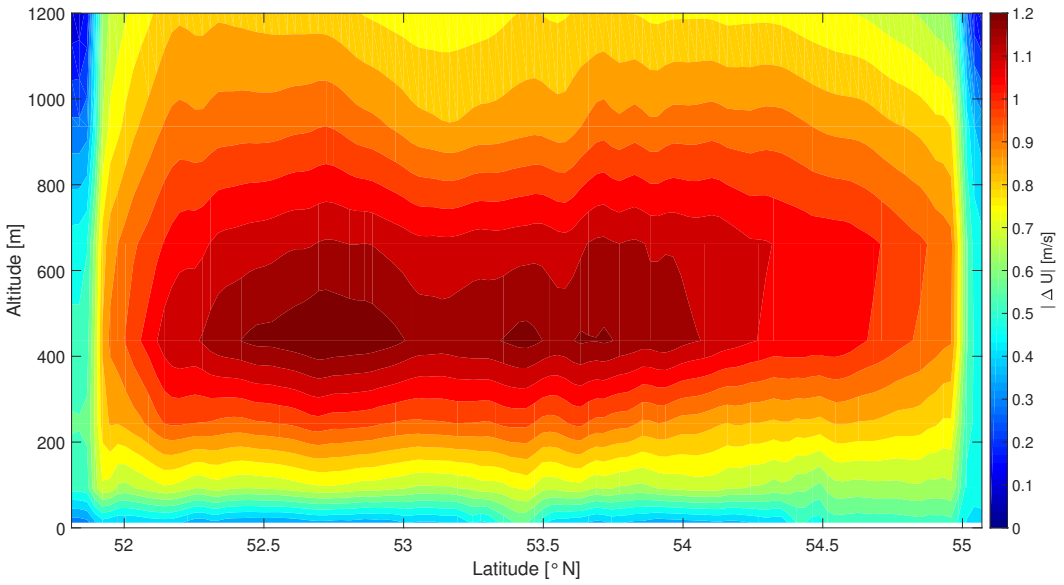

(a) Slice along constant longitude

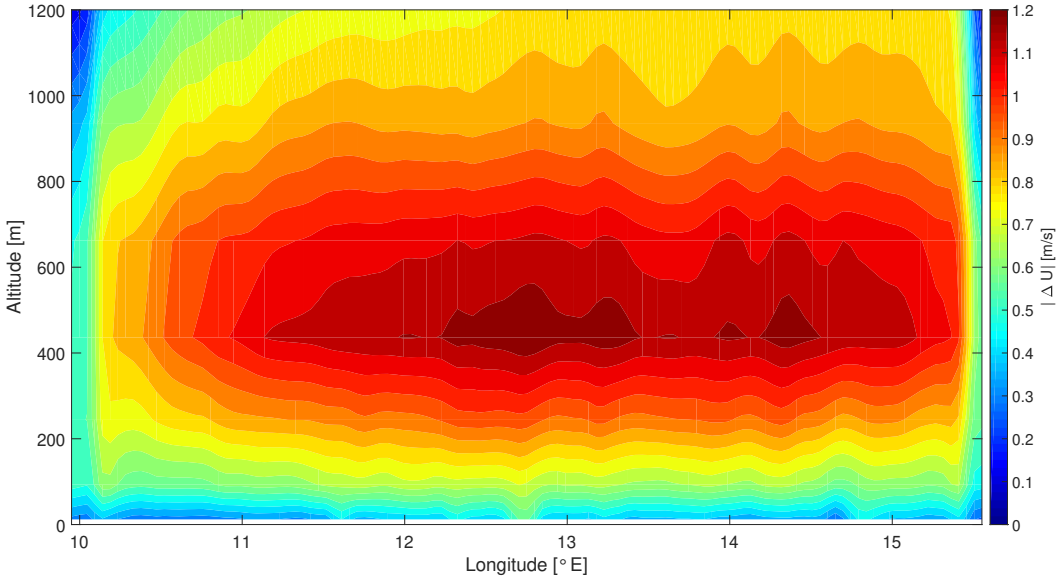

(b) Slice along constant latitude

Figure 7. ~~Absolute difference in horizontal wind speed $\Delta\overline{U_{WRF}}$ along lines of constant longitude (Lon: 12° 11' 20.98"E) and constant latitude (Lat: 53° 10' 47.00"N) through the center nudging point (i.e. the LiDAR measurement location).~~

4.4 Diurnal Variability

Average diurnal variation indicates typical wind speed variations for a given location and period. It further reinforces the benefit of dynamically adapting operating altitudes of AWES. The hourly average LiDAR wind speed depends on data availability

described in section 2. LiDAR availability below $100m$ on average decreases by about 10 percentage points during the noon hours, while it remains fairly constant at altitudes between $100m$ and $300m$. Above this altitude, data availability increases in the afternoon by up to about 15 percentage points (Sommerfeld et al., 2019).

Figure 8 shows the LiDAR measured and mesoscale modeled diurnal wind speed variation at the measurement location filtered by LiDAR availability, i.e. times where no LiDAR data were available were disregarded. A clear diurnal wind speed variation resulting from the cycle of stable and unstable stratification can be identified. On average OBS shows lower hourly wind speeds than NoOBS and is closer to measurements. The diurnal variation of the 6 months OBS, the 6 months NoOBS the 12 months NoOBS unfiltered data sets (Figure 9) deviate significantly from the measurements. Observation nudging leads to overall lower wind speeds and wind shear throughout the day in the unfiltered data set. Due to the large difference in average measured and unfiltered modeled diurnal wind speeds, it seems that LiDAR measurements alone can not appropriately represent average wind conditions aloft due to availability bias which also has been observed at other locations (Gryning and Floors, 2019). Therefore, we believe that the nudged data set yields more representative results than the unnudged model or the measurements alone.

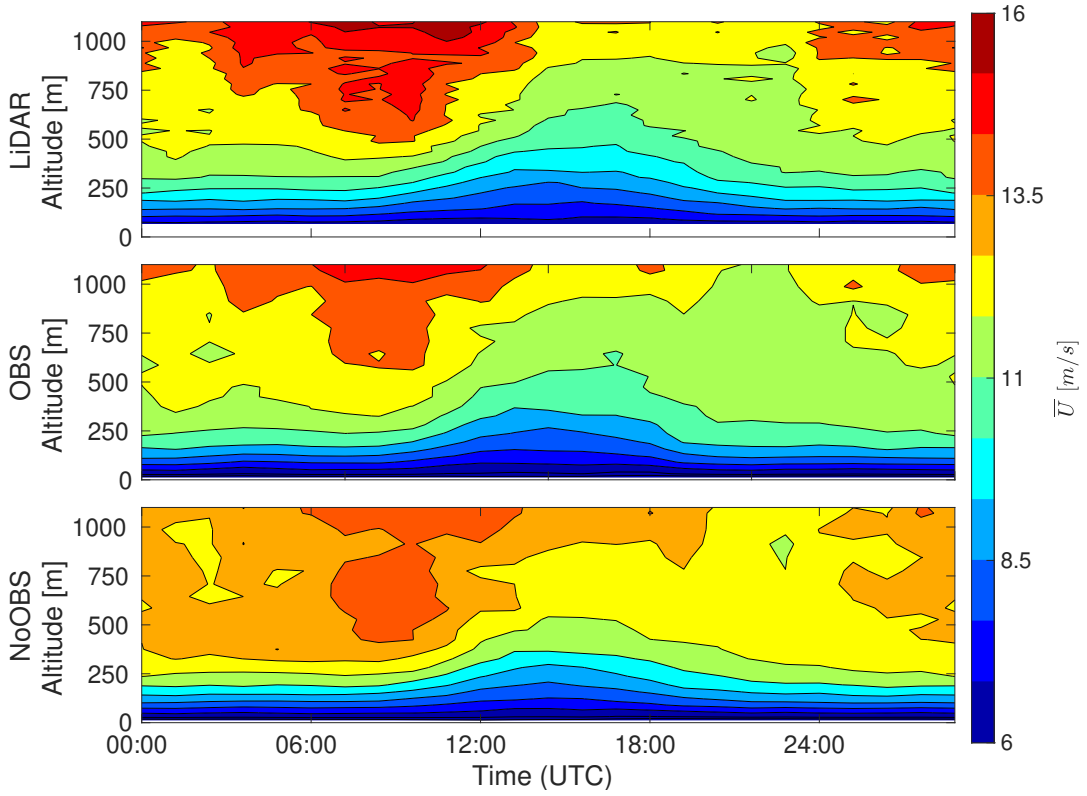

Figure 8. Hourly average diurnal variation of LiDAR measured (top), OBS (center) and NoOBS (bottom) modeled horizontal wind speed $\overline{U}$ filtered by LiDAR availability.

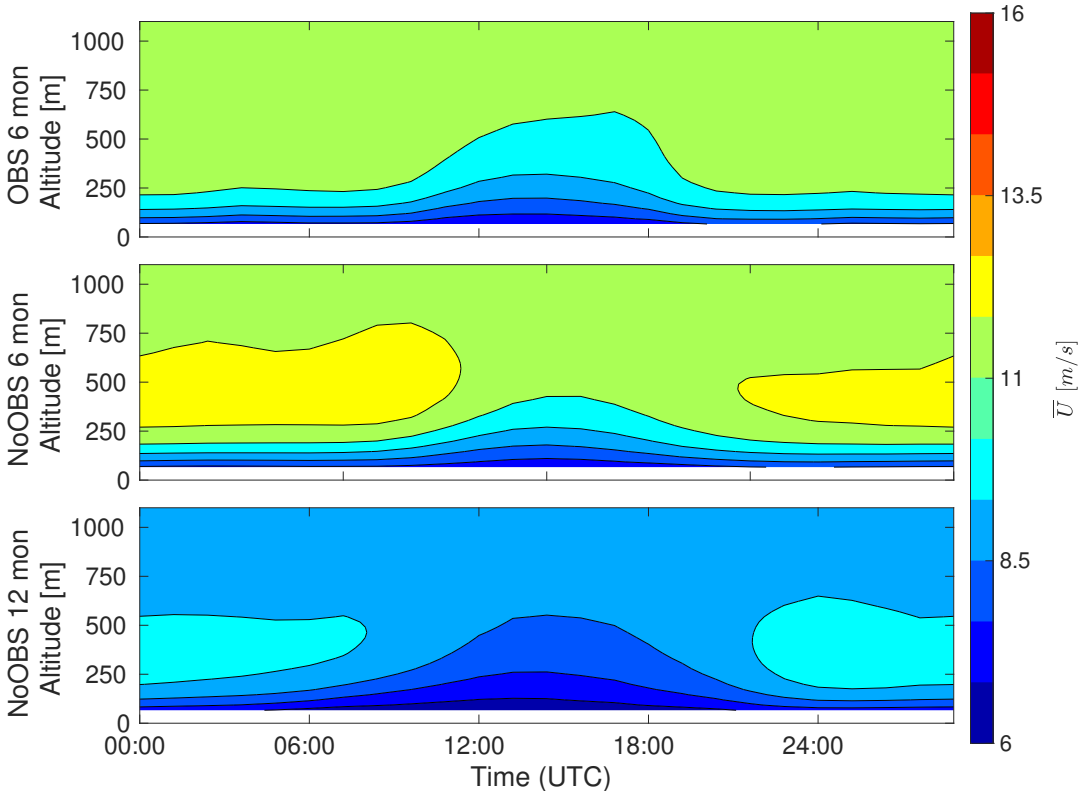

Figure 9. Hourly average diurnal variation of unfiltered OBS (top), 6 months NoOBS (center) and 12 months NoOBS (bottom) modeled horizontal wind speed $\overline{U}$ ~~filtered by LiDAR availability~~.

4.5 Wind speed probability distribution

The common way to approximate the probability distribution of the horizontal wind speed $f(U)$ is the *Weibull distribution fit* (eq. 3) which describes the statistical distribution as a function of the scale parameter A and the shape parameter k (Troen and Lundtang Petersen, 1989).

$$f_{Weibull}(u) = \frac{k}{A}\left(\frac{u}{A}\right)^{k-1} e^{-\left(\frac{u}{A}\right)^{k}} \tag{3}$$

Previous investigation of the LiDAR measurements showed a multi-modality in the wind speed probability distribution caused by different atmospheric stability (Sommerfeld et al., 2019). The left column in figure 10 visualizes the entire wind speed probability distribution. Its corresponding Weibull fit is shown in the center column and the difference between both can be found on the right hand side. Each row summarizes the various data sets first 6 months LiDAR, then 6 months OBS, 6 months NoOBS followed by 12 months NoOBS.

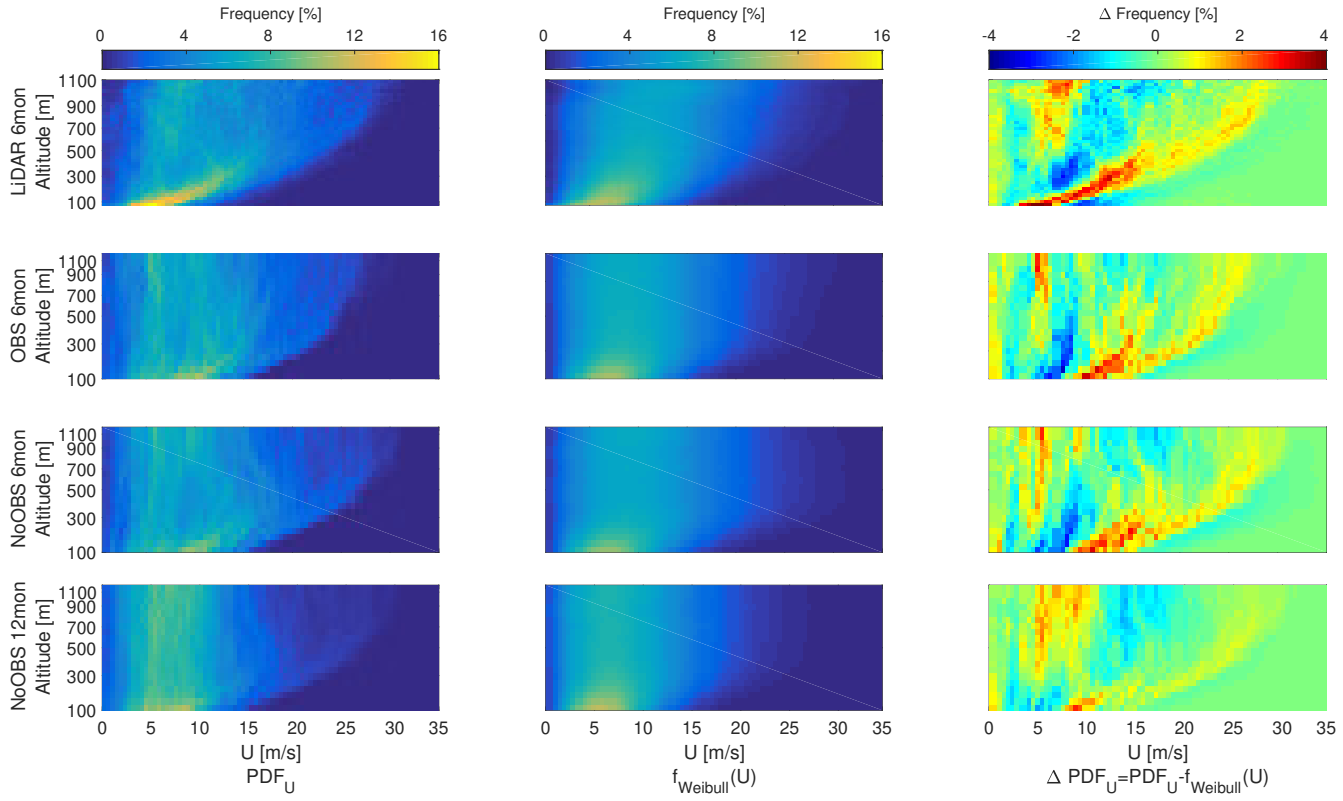

Figure 10. Probability distribution (left), Weibull fit (center) and difference between both (right) of 6 months LiDAR measurements (top row), 6 months OBS model (second row), 6 months NoOBS model (third row) and 12 months NoOBS (bottom row). The entire, (not filtered by LiDAR data availability) was used for the WRF data set.

All 6 months data sets show a high occurrence of low and high wind speeds which indicates a multi-modal probability distribution. This effect is most pronounced in the LiDAR data set. The comparison of wind speed PDF with the Weibull fit (right column) further emphasizes the multi-modality as a simple Weibull fit is not able to capture the higher probability at low and high wind speeds. These distinct flow situations further drift apart with increasing surface-distance. As a result the Weibull distribution overestimates the occurrence of wind speeds in between the two peaks (blue area in right column). Both OBS and NoOBS slightly overestimate low altitude wind speed (see figure 4) compared to LiDAR measurements. Both models and the LiDAR measurements show a broadening of the probability distribution towards higher altitudes. High wind speeds become more likely while low wind speeds still occur. Therefore, AWES need to be able to operate in a wide range of wind speeds or be controlled in a way that they avoid extreme conditions. The 12 months NoOBS simulation shows lower wind speeds than the 6 months simulations as the included summer months generally have lower wind speeds ~~due to higher probability of unstable stratification~~ due to the lower synoptic pressure gradients.

The Weibull fit of this simulation tends to overestimate higher wind speeds and underestimate low wind speeds at all altitudes.

~~We use the sign~~ Using the sign of the WRF-calculated SHF as a simple proxy to differentiate stable and unstable wind conditions similar to (Sommerfeld et al., 2019). The wind speed probability distribution follow the expected trends of low wind shear during unstable stratification and higher wind shear and wind speeds during stable stratification (Arya and Holton, 2001). Observation nudging reduces the occurrence of high wind speeds at high-altitudes in comparison to NoOBS and leads to an increase in the probability of wind speeds around 5 m/s during times of positive SHF. The Weibull distribution fit of these sub-states is generally better at representing the modeled wind conditions.

Figure 11 shows the scale parameter A, shape parameter k and Hellinger distance H (Upton and Cook, 2008) between the wind speed PDF and the corresponding Weibull distribution fit for LiDAR (1st row), 6 months OBS (2nd row), 6 months NoOBS (3rd row) and 12 months NoOBS (4th row).

The different trends under positive and and negative SHF of both Weibull parameters visualize the existence of entirely different flow regimes. The Hellinger distance between the Weibull fit and PDF (negative SHF: blue and positive SHF: red), the total data and a simple fit (black) as well as between the total data and the weighted sum of both Weibull fits (green) is shown in the right graph. All WRF models show an overall smaller H than a similar analysis of the LiDAR data set ~~(see~~ (Sommerfeld et al., 2019). The sharp bend in both A and k of the LiDAR data above 750 m is likely caused by insufficient data availability. NoOBS results show a sharp increase of A up to 250 m and a slight reduction above while OBS shows a trend close to the surface, A values remain almost constant above 500 m. No data set shows a convergence of A at higher altitudes indicating that these wind conditions are driven by different conditions in the free atmosphere. 12 months NoOBS simulations show lower scale parameter values as they include generally slower winds during summer. While A trends are quite different for LiDAR and WRF, k trends are more similar. They peak between 150 and 250 m and are especially high during stable stratification (Monahan et al., 2011). OBS trends of k are generally closer to measurement results than NoOBS.

Even though the Hellinger distance of individual Weibull fits for times of positive or negative SHF is generally higher than the Weibull fit of the entire data set, the weighted sum of both individual fits yields the best result at all altitudes.

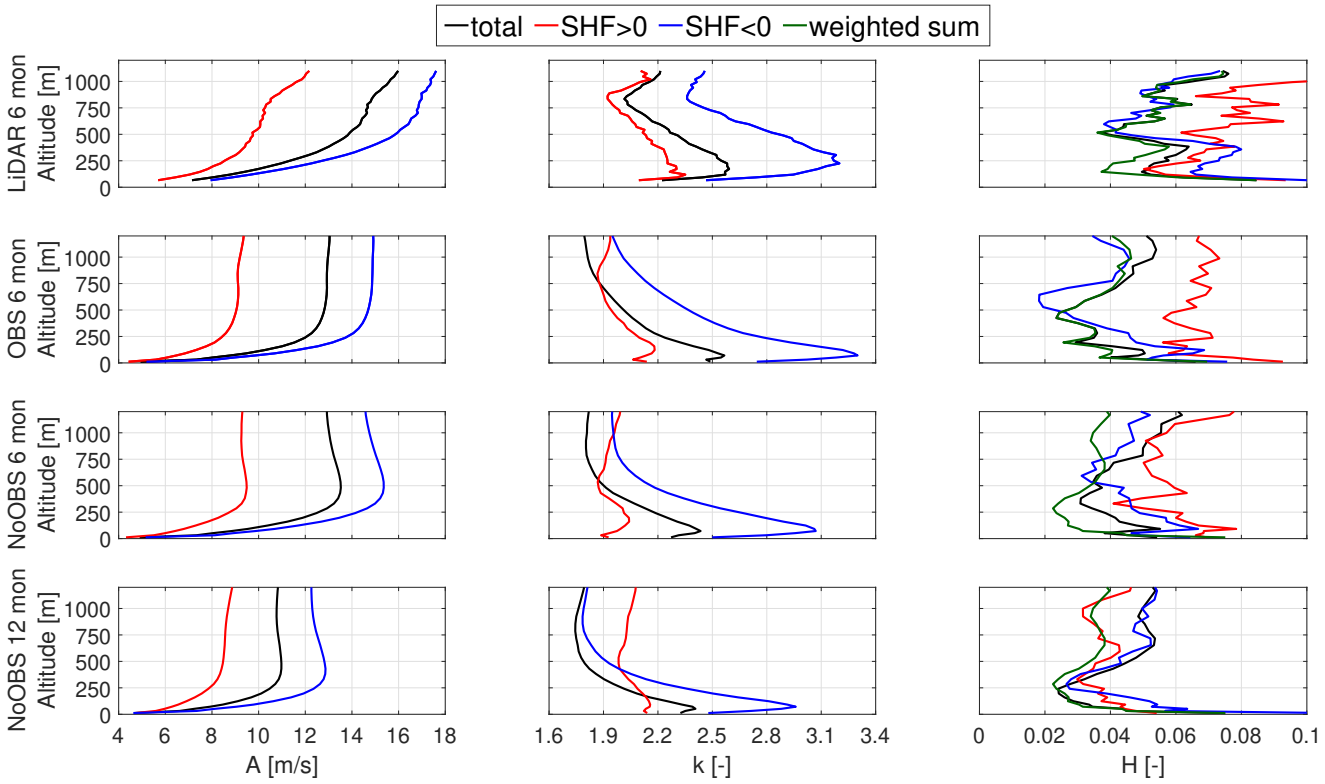

Figure 11. Weibull parameter trends over altitude and goodness of fit quantified by the Hellinger distance (right) over altitude for 6 months of LiDAR measurements (1st row), the 6 months OBS model (2nd row), 6 months NoOBS model (3rd row) and the 12 months NoOBS model (4th row)

4.6 Effect of stability on average wind shear

Atmospheric stability highly influences the shape of wind speed profiles which is important for determining optimal operating conditions for AWES (see section 4.7). ~~We quantify the impact of observation nudging on various~~ Stability classes were categorized based on ~~defined by~~ the Obukhov length OL (Obukhov, 1971) . ~~calculated from~~ OL is defined by the simulated friction velocity u_*, virtual potential temperature θ_v, potential temperature θ, kinematic virtual sensible surface heat flux Q_S, kinematic virtual latent heat flux Q_L, the von Kármán constant k and gravitational acceleration g. Table 3 summarizes the frequency of occurrence of each stability class.

$$L_{WRF} = \frac{-u_*^3 \theta}{kgH_{sfc}} \tag{4}$$

$$OL = \left(\frac{-u_*^3 \theta_v}{kg}\right)\left(\frac{1}{Q_S} + \frac{0.61}{Q_L \theta}\right) \tag{5}$$

Table 3 summarizes the Obukhov length bins and frequency of occurrence of each stability class.

Table 2. Stability classes according to Obukhov length (OL)calculated based on WRF results (Floors et al., 2011)

Stability classes	L [m]	# OBS 6 mon	# NoOBS 6 mon	# NoOBS 12 mon
Unstable (u)	$-200 \leq L_{WRF} \leq -100$	1509	1042	3827
Near unstable (nu)	$-500 \leq L_{WRF} \leq -200$	2121	1658	3736
Neutral (n)	$\lvert L_{WRF} \rvert \geq 500$	7342	7648	10756
Near stable (ns)	$200 \leq L_{WRF} \leq 500$	4791	4987	6590
Stable (s)	$50 \leq L_{WRF} \leq 200$	4862	4861	9114
Very stable (vs)	$10 \leq L_{WRF} \leq 50$	1567	1765	5306
Other	$-100 \leq L_{WRF} \leq 10$	3729	3960	13231

Table 3. Stability classes according to Obukhov length calculated based on WRF results (Floors et al., 2011)

Stability classes	L [m]	OBS 6 mon	NoOBS 6 mon	NoOBS 12 mon
Unstable (u)	$-200 \leq OL \leq -100$	5.8 %	4.0 %	7.3 %
Near unstable (nu)	$-500 \leq OL \leq -200$	8.2 %	6.4 %	7.1 %
Neutral (n)	$\lvert OL \rvert \geq 500$	28.3 %	29.5 %	20.5 %
Near stable (ns)	$200 \leq OL \leq 500$	18.5 %	19.2 %	12.5 %
Stable (s)	$50 \leq OL \leq 200$	18.8 %	18.8 %	17.3 %
Very stable (vs)	$10 \leq OL \leq 50$	6.0 %	6.8 %	10.1 %
Other	$-100 \leq OL \leq 10$	14.4 %	15.3 %	25.2 %

In comparison with the unnudged simulation, OBS shows an increase in unstable and near unstable situations. Stable and near stable stratification seems almost unaffected by OBS nudging, while neutral and very stable stratification occur slightly less often. This might improve the overall predicting capabilities of WRF as the MYNN 2.5 boundary layer scheme overestimates the frequency of very stable conditions with an error of up to 9 % (Krogsæter and Reuder, 2015). Neutral conditions, still commonly used in many wind energy siting applications, only occur about 30 % of the time during the measurement period and only about 20 % of the time during the one year reference NoOBS simulation.

Figure 12 shows the mean wind speed profiles categorized and normalized by the corresponding friction velocity u_*. We assumed that The nudged simulation OBS is assumed to be sufficiently close to the measurements and is therefore used to normalize and the same categorization as in OBS, since no measurements were available to determine L_{LiDAR}. All profiles follow expected trends with unstable profiles showing the smallest wind shear and stable profiles showing the largest. Altitudes below 200 m are least affected by observation nudging as OBS remains almost unchanged from NoOBS (see section 4.1). Both models are in good accordance with measurements during unstable and near unstable conditions. The stable and very stable profiles of the unnudged simulation show a peak at around 300 m which is indicative of a characteristic low level jet. The more irregular trend of the very stable LiDAR data set could be caused by a small sample size since only 5 % of the overall data is considered very stable.

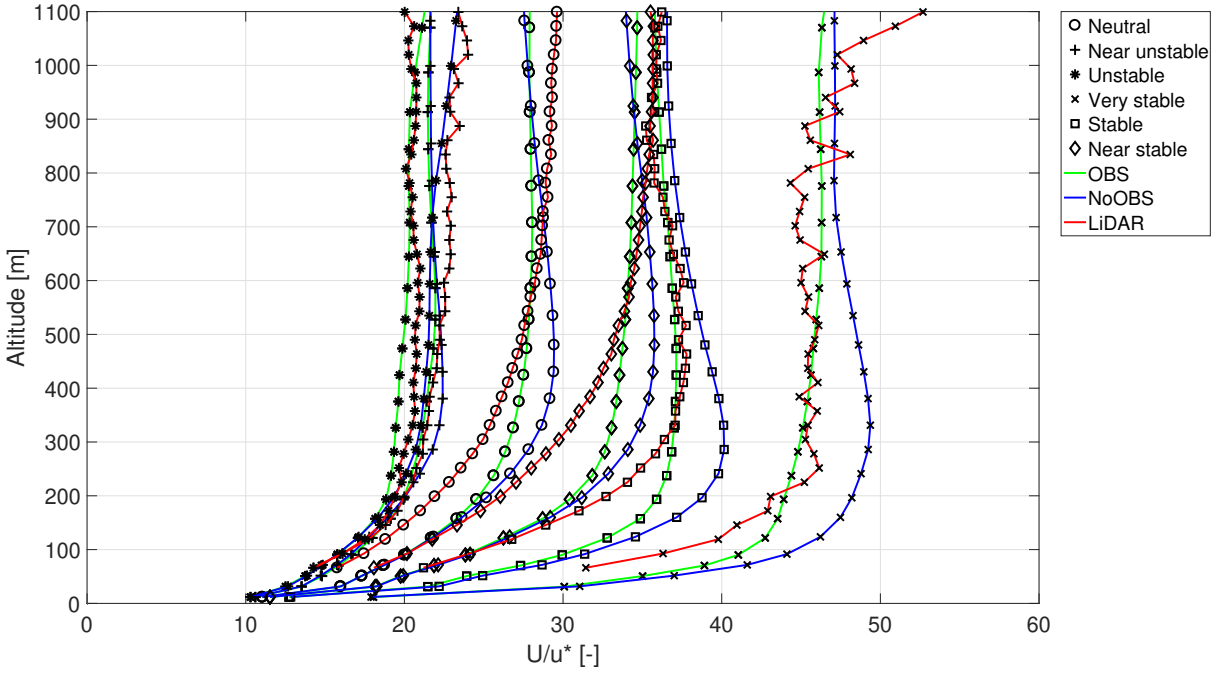

Figure 12. 6 months mean HWS profiles of LiDAR, OBS and NoOBS data classified by stability class defined by Obukhov length (table 3).

Expanding on the previous approach (subsection 4.5) of splitting the data into times of positive and negative SHF to differentiate states of unstable and stable stratification, we make use of k-means clustering (Lloyd, 1982) to identify two additional sub-states ; stable and very stable as well as unstable and shear driven. to better differentiate between the different flow situatio We chose To differentiate additional two sub-states which identify stable and very stable as well as unstable and shear driven conditions. LiDAR results for reference can be found in (Sommerfeld et al., 2019).

Figures 14 to ?? shows the probability distribution of each sub-state the different stability categories for each model simulation with the cluster centroids mean highlighted by white squares. All clusters categorize show distinct trends and distributions that are consistent between data sets , which contribute to the multi-modality of the overall wind speed probability

distribution. The difference in high-altitude wind speeds between stratifications indicate the influence of different geostrophic wind conditions. The categorization by OL is based on surface data and seems to be valid within the lower part of the atmosphere where the spread of the corresponding probability distribution is relatively small in comparison to high altitudes. This is particularly true for stable and neutral stratification where wind speeds above approximately 200 m spread widely. Unstable conditions are probably more consistent because of increased mixing up to high altitudes. Altitudes below 200 m are least affected by observation nudging as OBS remains almost unchanged from NoOBS (see section 4.1). Stable profiles show a peak at around 300 m which is indicative of a characteristic low level jet. Comparing OBS and NoOBS 6 months, observation nudging seems to reduce the spread at higher altitudes within each category except very stable. The impact of observation nudging on wind profiles during unstable stratification is relatively low while wind speed profiles under neutral and stable stratification are more affected. ~~The top left plot in each figure shows the probability distribution of a typical unstable stratification with low wind shear all the way up to 1100 m. The top right plot shows statistics of shear-driven wind profiles that occur during times of positive SHF. Stable (bottom right) and very stable stratification (bottom left) are characterized by strong wind shear and higher average wind speeds. NoOBS predicts a higher chance of wind speed reduction during very stable stratification above 600 m while wind speeds in OBS steadily increase up to 1100 m. Both models indicate the existence of LLJ during stable stratification between 200 and 400 m. The difference in high-altitude wind speeds indicate the influence of different geostrophic winds.~~

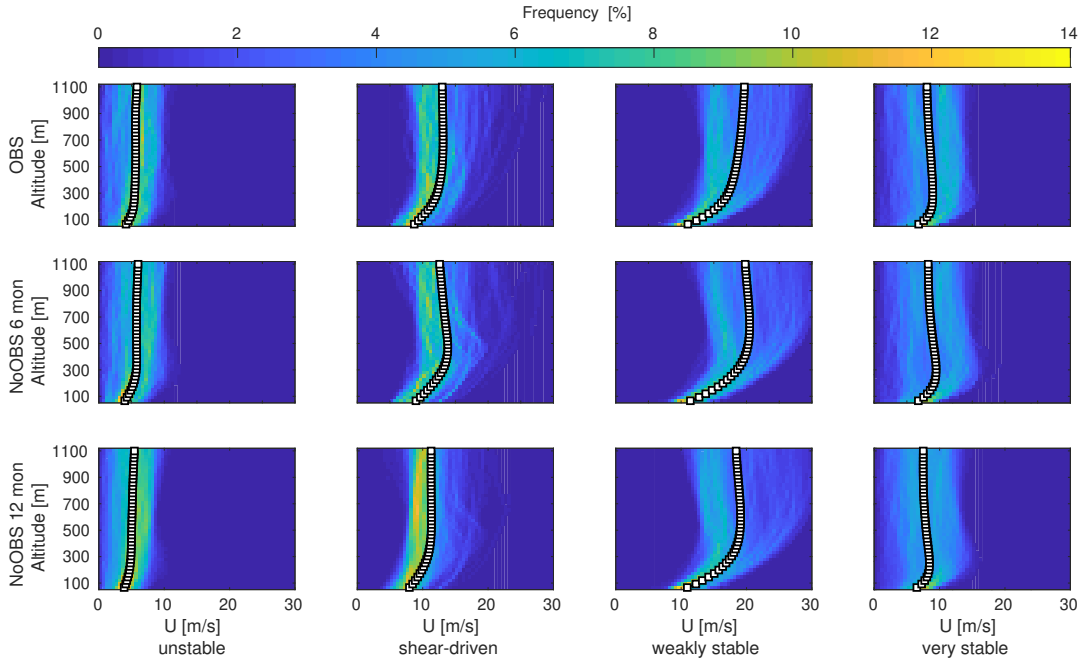

Figure 13. ~~Probability density function and mean (white square) of k-means clustered, SHF allocated OBS, 6 months NoOBS and 12 months NoOBS data. The two leftmost columns show times of positive SHF and the two rightmost columns times of negative SHF.~~

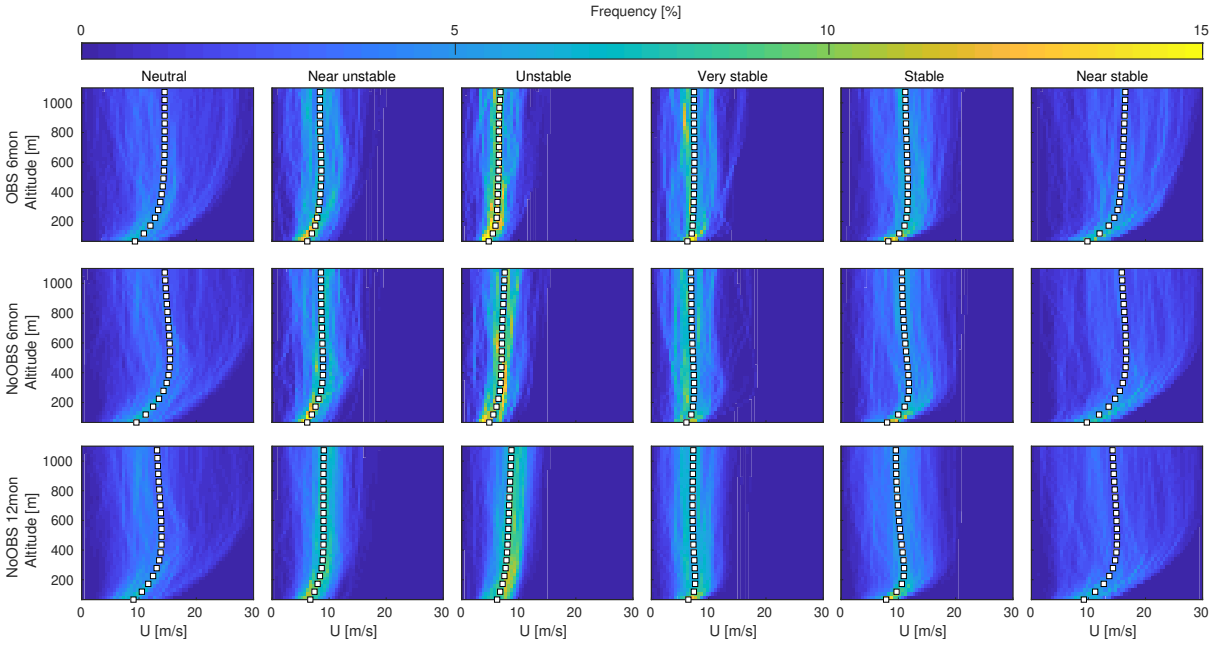

Figure 14. Probability density function and mean (white square) of OL categorized wind speeds for 6 months OBS, 6 months NoOBS and 12 months NoOBS data.

4.7 Optimal operating altitude and power production

We estimate optimal operating altitude and traction power of a ground-generator AWES using a simple ground-generator (pumping-mode) AWES point-mass model adapted from (Schmehl et al., 2013). We focus on 6 months OBS as we previously proved increased accuracy and use 12 months NoOBS to estimate annual values. The estimated optimal power per unit lifting area of the wing p_{opt} is described by:

$$p_{opt} = \frac{\rho_{air}}{2} U^3 \sqrt{c_L^2 + c_D^2} \left[1 + \left(\frac{c_L}{c_D}\right)^2\right] f_{opt} \left(\cos\varepsilon \cos\phi - f_{opt}\right)^2 = \frac{2}{27} \rho_{air} U^3 \sqrt{c_L^2 + c_D^2} \left[1 + \left(\frac{c_L}{c_D}\right)^2\right] \cos\varepsilon^3 \tag{6}$$

Air density ρ_{air} is calculated by a linear approximation of the standard atmosphere (ISO 2533:1975) ($\rho_{air}(z) = 1.225 - 0.00011z$ [kgm^{-3}]. Losses associated with ~~misalignment of~~ mispositioning of the aircraft relative to the wind direction ~~and the aircraft position~~ , expressed by azimuth angle ϕ and elevation angle ε relative to the ground station, are included in the model. Additional losses caused by gravity , tether sagging and tether drag are neglected. As a result, lift F_L and drag F_D force and therefore lift (c_L =1.7) ~~and drag coefficient~~ and drag coefficient (c_D =0.06) , which are assumed to be constant, are geometrically related to the ~~radial ($v_{a,r} = (\cos\varepsilon\cos\phi - f)U$) and tangential ($v_{a,t} = (\cos\varepsilon\cos\phi - f)U\frac{F_L}{F_D}$)~~ apparent wind velocity ~~components~~. ~~The tether speed v_t is non-dimensionalized in the form of the reeling factor ($f = \frac{v_t}{U}$).~~ Assuming an optimal ~~non-dimensional reeling factor~~ tether speed ~~($f_{opt} = \frac{1}{3}\cos\varepsilon\cos\phi$)~~ and a quasi-steady state with the wing moving directly cross-wind with a zero azimuth angle ($\phi = 0$) relative to the wind direction we can estimate the optimal traction power.

Optimal elevation angle (ε_{opt}) and operating altitude (z_{opt}) are geometrically related to the assumed to be constant tether length (L_{tether}) ($\sin\varepsilon_{opt} = \frac{z_{opt}}{L_{tether}}$).

Figure 16 summarizes the probability distribution of optimal operating altitude and optimal power assuming a constant tether length of 1500 m. ~~with~~ The white solid line shows~~ing~~ the cumulative frequency of optimal operating altitude. Both simulations for this particular location and time period show similar trends with the most probable optimal altitude between approximately 200 and 400 m. Times of very high traction power are fairly rare and likely associated with low level jets. Lower power at higher altitudes is caused by the misalignment losses. ~~Here we assume a constant tether length of 1500 m.~~

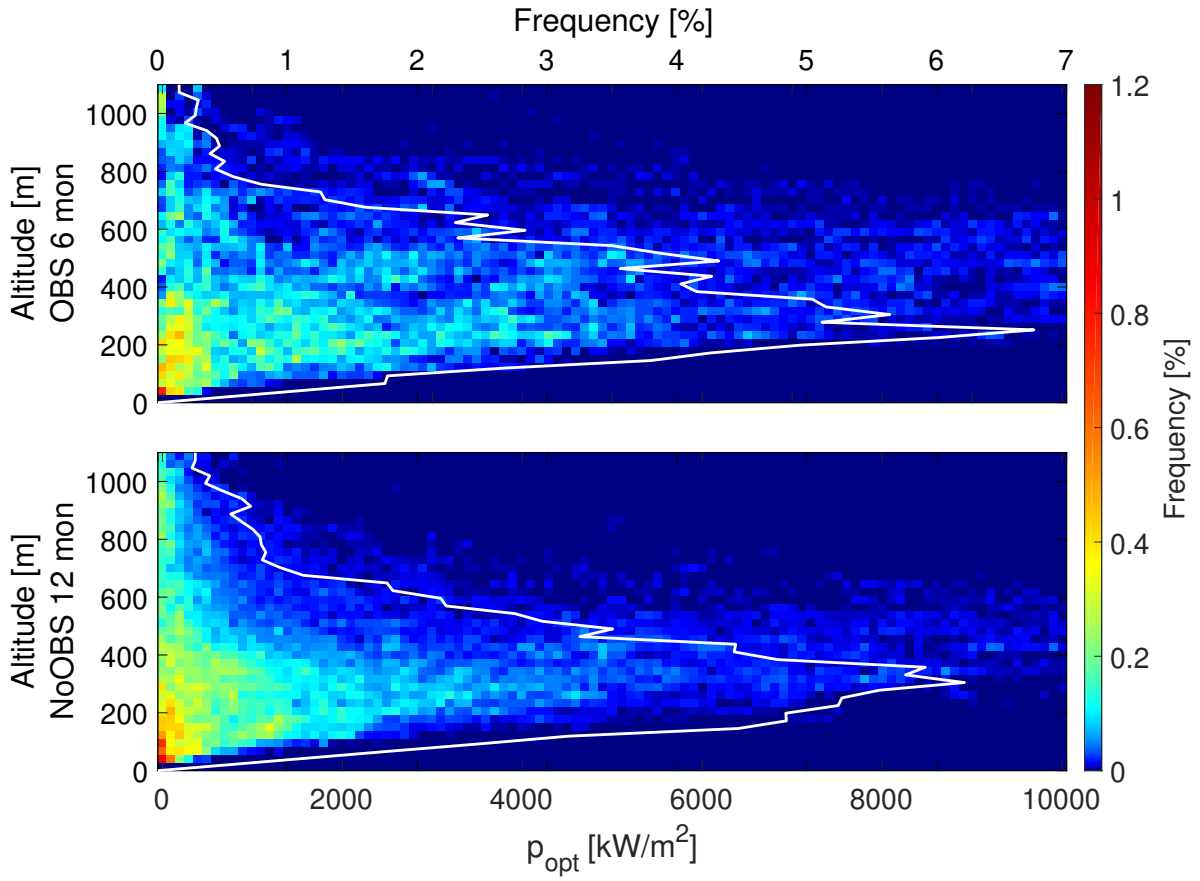

Figure 15. ~~Probability of optimal traction power over optimal operating altitude based on a) 6 months LiDAR, b) 6 months OBS, c) 6 months NoOBS and d) 12 months NoOBS. The continuous white line shows the frequency of optimal operating altitude for the whole power range (top abscissa axis).~~

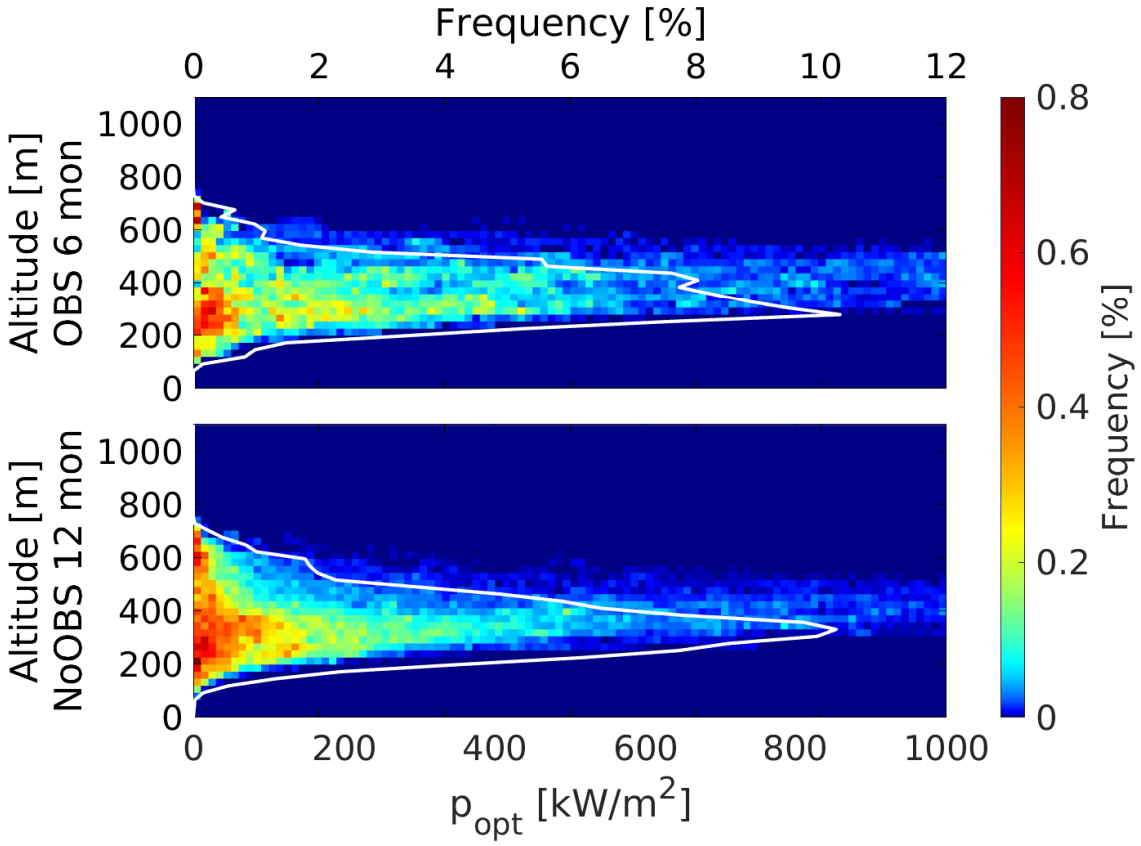

Figure 16. Probability of optimal traction power over optimal operating altitude based on 6 months OBS (top) and 12 months NoOBS (bottom) assuming a constant tether length of 1500 m. The continuous white line shows the frequency of optimal operating altitude for the whole power range (top abscissa axis).

Figure 18 estimates the optimal traction power and operating altitude as a function of tether length based on the mean wind speed profile of atmospheric stability condition (figure: 14) ~~clustered average profiles shown in figure 14~~. The tether length of each estimation is assumed to be constant and used to calculate the optimal elevation angle. The axis limits of different atmospheric conditions had to be adjusted as the calculated power varied in order of magnitudes. All estimates show diminishing benefits of a longer tether. These incremental gains would probably be negated by additional drag and weight associated losses. Winds during times of very stable and unstable stratification lead to a clear optimal altitude independent of tether length between 200 and 400 m while weakly stable and shear-driven wind speed profiles lead to higher optimal operating altitudes and a broader range of optimal altitudes as a function of tether length.

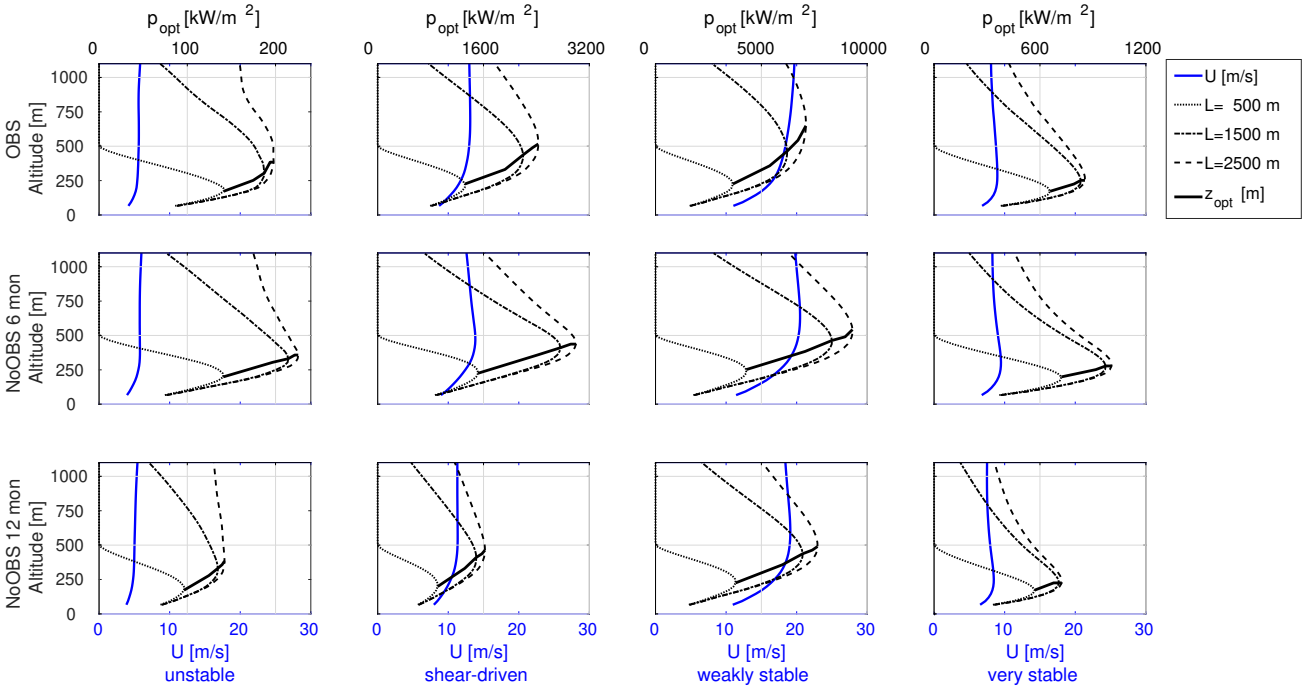

Figure 17. ~~Optimal traction power per wing area p_{opt} (dashed lines) and optimal operational altitude (solid line) estimated based on mean k-means-clustered SHF-sampled wind speed profiles of 6 months OBS, 6 months NoOBS and 12 months NoOBS simulation for varying tether length (L = 500 - 2500m)~~

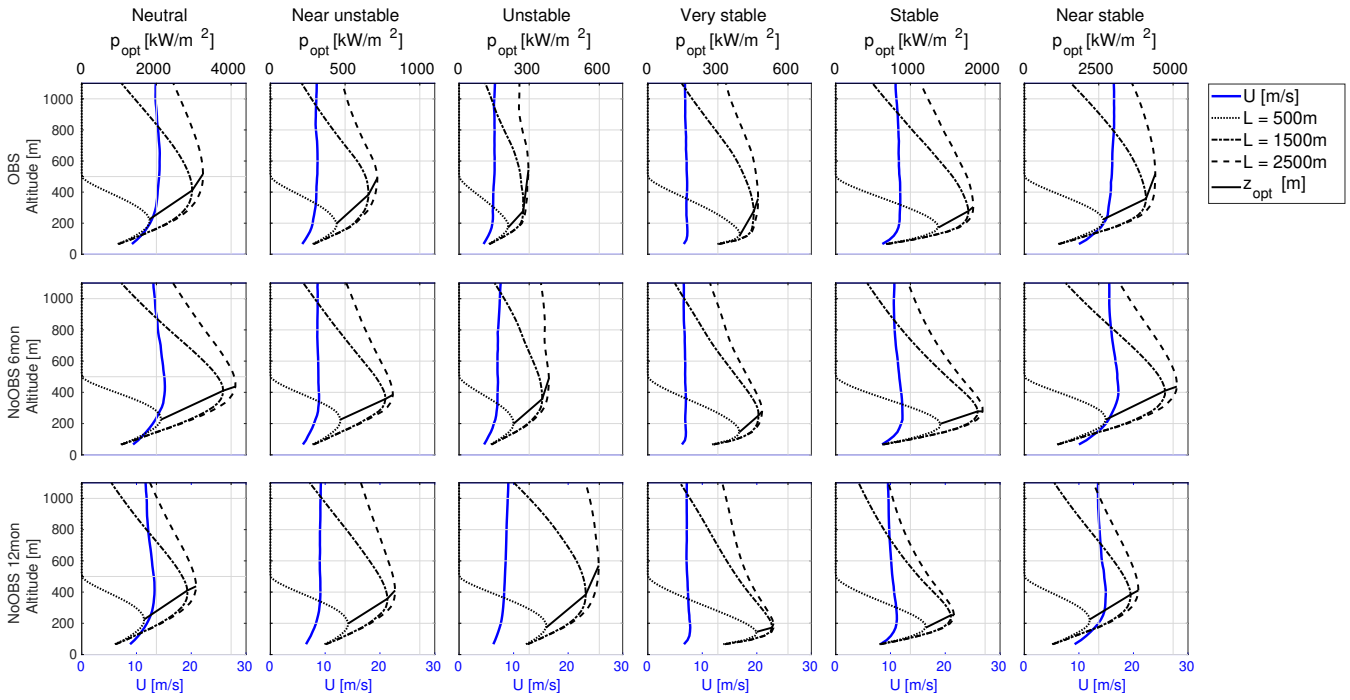

Figure 18. Optimal traction power per wing area p_{opt} (dashed lines) and optimal operational altitude (solid line) estimated based on mean wind speed profiles categorized by Obukhov length (OL) for 6 months OBS, 6 months NoOBS and 12 months NoOBS simulation with varying tether length (L = 500 - 2500m)

5 Conclusion

Six months of LiDAR measurements up to 1100 m were assimilated into a mesoscale model ~~WRF~~ using observation nudging. An unnudged reference model (NoOBS), the nudged model (OBS) outputs and LiDAR measurements were compared in terms of wind speed and direction statistics, wind profile shape at the measurement site as well as spatial differences were quantified. Observation nudging only has marginal impact on simulated surface layer wind speeds as ground effects dominate the WRF model. Wind speeds between 300 and 500 m were most affected by observation nudging. Modeled wind speeds at these altitudes are statistically closest to measurements, making this an ~~excellent~~ adequate approach for resource assessment of mid-altitudes ~~wind energy systems~~ as measurement availability decreases. The impact of nudging weakens above these altitudes. Whether this is caused by lower measurement data availability or a generally ~~higher~~ better performance of the mesoscale model above the surface layer could not be determined. Observation nudging reduced the seemingly systematic wind direction bias between simulation and measurements at all altitudes. Due to the lack of high-resolution measurements at high-altitudes, unnudged mesoscale model data present the best we have got in terms of preliminary resource assessment.

Filtering the mesoscale model data according to LiDAR data availability yields similar diurnal variation with OBS being closer to measurements. Comparing the diurnal variation of the unfiltered model wind speeds to measurements shows

a significant deviation which is likely caused by insufficient LiDAR data availability at higher altitudes. The bias between real and LiDAR measured wind speed, which depends on the applied CNR threshold and data availability, can result in a misrepresentation of the actual wind conditions especially at higher altitudes. Mesoscale models, particularly with observation nudging, can be used to account for this error. LiDAR measurements seem to be biased towards high wind speeds as measured winds are generally higher than the unfiltered mesoscale model data. The impact of observation nudging on the wind profiles in case of an unstably stratified boundary layer is relatively low while wind speed profiles under stable stratification are significantly affected. ~~and~~ At the measurement location OBS is overall closer to measurements especially between 200 and 600 m. Variations of stratification, primarily those associated with the diurnal cycle, lead to a multi-modal wind speed probability distribution which is better represented by the weighted sum of two Weibull fits than by a single Weibull fit.

Optimal AWES operating altitudes and power output per wing area were estimated based on a simplified model for six months of OBS and twelve months of NoOBS. The model neglects kite and tether weight as well as tether drag. Accounting for these losses, which are proportional to tether length, will reduce the performance of the AWES. Results for both wind speed data sets show the highest potential at an altitude between 200 and 600 m above which the losses associated with the elevation angle are too high. A comparison of different tether lengths under average wind speeds associated with different atmospheric stability conditions show diminishing returns in terms of power output for tether lengths longer than 1500 m. While higher altitudes can be potentially be reached, optimal operating altitude remains almost unchanged. The highest energy potential and operating altitude is associated neutral and stable stratification. Unstable conditions result in significantly lower energy potential due to lower, almost altitude independent average wind speeds.

~~Using a simplified AWES model , assuming a constant tether length of 1500 m and neglecting drag and weight all data sets suggested an optimal operating altitude between 150 and 400 m. However, since stratification leads to a vast range of wind speed profiles AWES greatly benefit from dynamically adapting their operating altitude to maximize power production and minimize losses.~~

Future studies include using the enhanced mesoscale model output to drive large-eddy simulations, to provide a better insight into mid-altitude turbulence. The resulting data set will lead to the development of a mid-altitude engineering ~~(spectral)~~ wind model which can be used for design, load estimation, control and optimization of Airborne Wind Energy Systems. Mesoscale model data ~~could~~ will be implemented into an AWES optimization framework to quantify the impact of various wind speed profiles on power production, optimal trajectory and system size. Furthermore, the possibility of merging the mesoscale output with LiDAR measurements to fill gaps in the measurement data set to reduce the wind speed bias introduced by LiDAR availability is being investigated.

6 Appendix

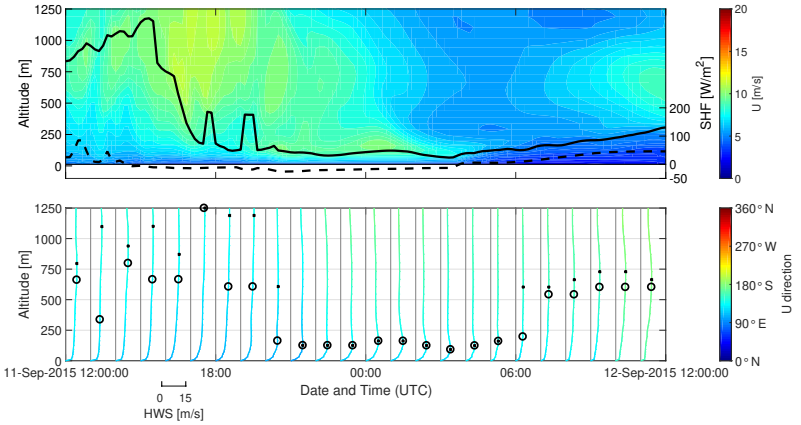

(a) NoOBS

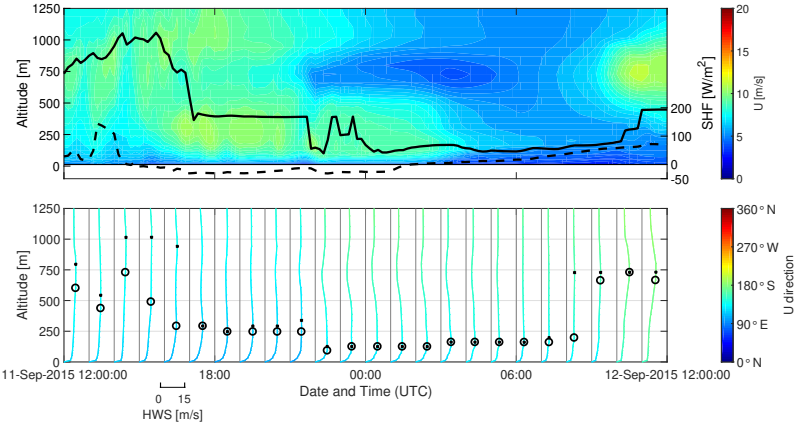

(b) OBS

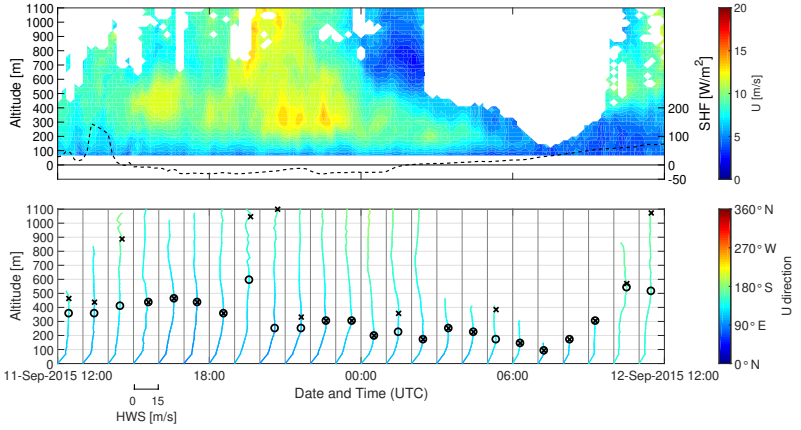

(c) LiDAR

Figure A1. ~~Contour plot and U profile; instead plot contour plots beneath each other and all profiles in 1 plot?~~

Table A1. Namelist parameters for WRF 3.6.1 observation nudging ~~settings~~

WRF input parameter	value
grid_fdda	1,1,1,
gfdda_inname	"wrffdda_d<domain>",
gfdda_end_h	99999, 99999, 99999,
gfdda_interval_m	360, 360, 360,
fgdt	0, 0, 0,
if_no_pbl_nudging_uv	0, 0, 1,
if_no_pbl_nudging_t	0, 0, 1,
if_no_pbl_nudging_q	0, 0, 1,
if_zfac_uv	0, 0, 0,
k_zfac_uv	0, 0, 30,
if_zfac_t	0, 0, 0,
k_zfac_t	0, 0, 30,
if_zfac_q	0, 0, 0,
k_zfac_q	0, 0, 30,
guv	0.0003, 0.0003, 0.0003,
gt	0.0003, 0.0003, 0.0003,
gq	0.0003, 0.0003, 0.0003,
if_ramping	1,
dtramp_min	60.0,
io_form_gfdda	2,

WRF input parameter	value
obs_nudge_opt	0,0,1
Cressman Scheme	1
time_step	60
obs_rinxy	240,240,180
obs_rinsig	0.1
obs_twindo	3, 3,3
auxinput11_interval_s	360, 360, 360
obs_dtramp	40
obs_nudge_wind	1,1,1
obs_coef_wind	6.E-4,6.E-4,6.E-4
iobs_onf	2,2,2
auxinput11_interval_s	360, 360, 360
auxinput11_end_h	6, 6, 6
if_no_pbl_nudging_uv	0, 0, 1
if_zfac_uv (max_dom)	0,0,30
sf_sfclay_physics	5, 5, 5
sf_surface_physics	4, 4, 4
bl_pbl_physics (max_dom)	5, 5, 5
bl_mynn_tkeadvect	.true.,.true.,.true.
ra_lw_physics	1 ,1,1
ra_sw_physics	1 ,1,1
mp_physics	5, 5, 5

Competing interests. The corresponding author (Markus Sommerfeld) confirms on behalf of all authors that there have been no involvements that might raise the question of bias in the work reported or in the conclusions, implications, or opinions stated.

Acknowledgements. The authors thank the federal ministry for economic affairs and energy for funding of the "OnKites I" and "OnKites II" project [grant number 0325394A] on the basis of a decision by the German Bundestag and project management Projektträger Jülich. The simulations were performed at the HPC Cluster EDDY, located at the University of Oldenburg (Germany) and funded by the federal ministry for economic a under grant number 0324005. We thank the PICS and the DAAD for their funding. We further thank all the technicians and staff at IWES for carrying out the measurement campaign at Pritzwalk and their support in evaluating the data.

References

Al-Yahyai, S., Charabi, Y., and Gastli, A.: Review of the use of numerical weather prediction (NWP) models for wind energy assessment, Renewable and Sustainable Energy Reviews, 14, 3192–3198, doi:10.1016/j.rser.2010.07.001, 2010.

Archer, C. L. and Caldeira, K.: Global Assessment of High-Altitude Wind Power, Energies, 2, 307–319, doi:10.3390/en20200307, 2009.

Arya, P. and Holton, J.: Introduction to Micrometeorology, International Geophysics, Elsevier Science, 2001.

Bastigkeit, I., Gottschall, J., Gambier, A., Sommerfeld, M., Wolken-Möhlmann, G., and Rudolph, C.: Abschlussbericht-OnKites-Juni 2017_Final-5, detailled report AP1-AP2-AP5, Fraunhofer-Institut für Windenergie und Energiesystemtechnik IWES Nordwest, Bremerhaven, 2017.

Bechtle, P., Schelbergen, M., Schmehl, R., Zillmann, U., and Watson, S.: Airborne wind energy resource analysis, Renewable Energy, 141, 1103 – 1116, doi:https://doi.org/10.1016/j.renene.2019.03.118, 2019.

Brunner, D., Savage, N., Jorba, O., Eder, B., Giordano, L., Badia, A., Balzarini, A., Baró, R., Bianconi, R., Chemel, C., Curci, G., Forkel, R., Jiménez-Guerrero, P., Hirtl, M., Hodzic, A., Honzak, L., Im, U., Knote, C., Makar, P., Manders-Groot, A., van Meijgaard, E., Neal, L., Pérez, J. L., Pirovano, G., San Jose, R., Schröder, W., Sokhi, R. S., Syrakov, D., Torian, A., Tuccella, P., Werhahn, J., Wolke, R., Yahya, K., Zabkar, R., Zhang, Y., Hogrefe, C., and Galmarini, S.: Comparative analysis of meteorological performance of coupled chemistry-meteorology models in the context of AQMEII phase 2, Atmospheric Environment, 115, 470–498, doi:10.1016/j.atmosenv.2014.12.032, 2015.

Burton, T., ed.: Wind energy handbook, Wiley, Chichester, West Sussex, 2nd ed edn., doi:10.1002/9781119992714, 2011.

Canut, G., Couvreux, F., Lothon, M., Legain, D., Piguet, B., Lampert, A., Maurel, W., and Moulin, E.: Turbulence fluxes and variances measured with a sonic anemometer mounted on a tethered balloon, Atmospheric Measurement Techniques, 9, 4375–4386, doi:10.5194/amt-9-4375-2016, 2016.

Carvalho, D., Rocha, A., Gómez-Gesteira, M., and Silva Santos, C.: WRF wind simulation and wind energy production estimates forced by different reanalyses: Comparison with observed data for Portugal, Applied Energy, 117, 116–126, doi:10.1016/j.apenergy.2013.12.001, 2014.

Cherubini, A., Papini, A., Vertechy, R., and Fontana, M.: Airborne Wind Energy Systems: A review of the technologies, Renewable and Sustainable Energy Reviews, 51, 1461–1476, doi:10.1016/j.rser.2015.07.053, 2015.

Dee, D. P., Uppala, S. M., Simmons, A. J., Berrisford, P., Poli, P., Kobayashi, S., Andrae, U., Balmaseda, M. A., Balsamo, G., Bauer, P., Bechtold, P., Beljaars, A. C. M., van de Berg, L., Bidlot, J., Bormann, N., Delsol, C., Dragani, R., Fuentes, M., Geer, A. J., Haimberger, L., Healy, S. B., Hersbach, H., Hólm, E. V., Isaksen, L., Kållberg, P., Köhler, M., Matricardi, M., McNally, A. P., Monge-Sanz, B. M., Morcrette, J.-J., Park, B.-K., Peubey, C., de Rosnay, P., Tavolato, C., Thépaut, J.-N., and Vitart, F.: The ERA-Interim reanalysis: configuration and performance of the data assimilation system, Quarterly Journal of the Royal Meteorological Society, 137, 553–597, doi:10.1002/qj.828, 2011.

Deng, A., Stauffer, D. R., Dudhia, J., Otte, T., and Hunter, G. K.: Update on analysis nudging FDDA in WRF-ARW, in: Proceedings of the 8th WRF Users' Workshop, p. 35, 2007.

Dudhia, J.: WRF Four-Dimensional Data Assimilation (FDDA), http://www2.mmm.ucar.edu/wrf/users/tutorial/200801/WRF_FDDA_Dudhia.pdf, 2012.

Fagiano, L. and Milanese, M.: Airborne Wind Energy: An overview, in: 2012 American Control Conference (ACC), pp. 3132–3143, IEEE, doi:10.1109/ACC.2012.6314801, 2012.

Fechner, U. and Schmehl, R.: Flight Path Planning in a Turbulent Wind Environment, in: Airborne Wind Energy: Advances in Technology Development and Research, edited by Schmehl, R., pp. 361–390, Springer Singapore, Singapore, doi:10.1007/978-981-10-1947-0_15, 2018.

Floors, R., Batchvarova, E., Gryning, S.-E., Hahmann, A. N., Peña, A., and Mikkelsen, T.: Atmospheric boundary layer wind profile at a flat coastal site - wind speed lidar measurements and mesoscale modeling results, Advances in Science and Research, 6, 155–159, doi:10.5194/asr-6-155-2011, 2011.

Gambier, A., Bastigkeit, I., and Nippold, E.: Projekt OnKites II: Untersuchung zu den Potentialen von Flugwindenergieanlagen (FWEA) Phase II : Abschlussbericht (ausführliche Darstellung), Fraunhofer Institut für Windenergie und Energiesystemtechnik, https://doi.org/10.2314/GBV:1009915452, 2017.

Giannakopoulou, E.-M. and Nhili, R.: WRF Model Methodology for Offshore Wind Energy Applications, Advances in Meteorology, 2014, 1–14, doi:10.1155/2014/319819, 2014.

Gottschall, J.: GALION LIDAR PERFORMANCE VERIFICATION, technical report, Fraunhofer-Institut für Windenergie und Energiesystemtechnik IWES Nordwest, Bremerhaven, https://www.woodgroup.com/__data/assets/pdf_file/0023/15692/report_Sgurr_20130529_FINAL1.pdf, 2013.

Gottschall, J., Lindelöw-Marsden, P., and Courtney, M.: Executive summary of key test results for SgurrEnergy Galion, Executive summary, Technical University of Denmark DTU, Roskilde, https://www.woodgroup.com/__data/assets/pdf_file/0024/15693/Riso_ExecutiveSummary_-Galion_lidar.pdf, 2009.

Gryning, S.-E. and Floors, R.: Carrier-to-Noise-Threshold Filtering on Off-Shore Wind Lidar Measurements, Sensors, 19, 592, 2019.

IEC, I.: 61400-1: Wind turbines part 1: Design requirements, International Electrotechnical Commission, p. 177, 2005.

ISO 2533:1975: Standard Atmosphere, Standard, International Organization for Standardization, Geneva, CH, 1975.

Krogsæter, O. and Reuder, J.: Validation of boundary layer parameterization schemes in the Weather Research and Forecasting model (WRF) under the aspect of offshore wind energy applications - Part II: Boundary layer height and atmospheric stability, Wind Energy, 18, 1291–1302, doi:10.1002/we.1765, 2015.

Lee, J. C. Y. and Lundquist, J. K.: Observing and Simulating Wind-Turbine Wakes During the Evening Transition, Boundary-Layer Meteorology, 164, 449–474, doi:10.1007/s10546-017-0257-y, 2017.

Lloyd, S.: Least squares quantization in PCM, IEEE Transactions on Information Theory, 28, 129–137, doi:10.1109/TIT.1982.1056489, 1982.

Lunney, E., Ban, M., Duic, N., and Foley, A.: A state-of-the-art review and feasibility analysis of high altitude wind power in Northern Ireland, Renewable and Sustainable Energy Reviews, 68, 899 – 911, doi:https://doi.org/10.1016/j.rser.2016.08.014, 2017.

Mann, J.: The spatial structure of neutral atmospheric surface-layer turbulence, Journal of Fluid Mechanics, 273, 141–168, doi:10.1017/S0022112094001886, 1994.

Mass, C. and Ovens, D.: WRF Model Physics: Problems and Progress, 2010.

Mass, C. and Ovens, D.: Fixing WRF's High Speed Wind Bias: A New Subgrid Scale Drag Parameterization and the Role of Detailed Verification, 2011.

Matthias, V. and Bösenberg, J.: Aerosol climatology for the planetary boundary layer derived from regular lidar measurements, Atmospheric Research, 63, 221 – 245, doi:https://doi.org/10.1016/S0169-8095(02)00043-1, 2002.

Monahan, A. H., He, Y., McFarlane, N., and Dai, A.: The Probability Distribution of Land Surface Wind Speeds, Journal of Climate, 24, 3892–3909, doi:10.1175/2011JCLI4106.1, 2011.

Mylonas-Dirdiris, M., Barbouchi, S., and Herrmann, H.: Mesoscale modelling methodology based on nudging to reduce the error of wind resource assessment, Conference: European Geosciences Union General Assembly at: Vienna, Austria, 2016.

Nakanishi, M. and Niino, H.: An Improved Mellor–Yamada Level-3 Model with Condensation Physics: Its Design and Verification, Boundary-Layer Meteorology, 112, 1–31, doi:10.1023/B:BOUN.0000020164.04146.98, 2004.

Obukhov, A. M.: Turbulence in an atmosphere with a non-uniform temperature, Boundary-Layer Meteorology, 2, 7–29, doi:10.1007/BF00718085, 1971.

Optis, M., Monahan, A., and Bosveld, F. C.: Limitations and breakdown of Monin–Obukhov similarity theory for wind profile extrapolation under stable stratification, Wind Energy, 19, 1053–1072, doi:10.1002/we.1883, 2016.

Peña, A., Gryning, S.-E., and Floors, R.: Lidar observations of marine boundary-layer winds and heights: a preliminary study, Meteorologische Zeitschrift, 24, 581–589, doi:10.1127/metz/2015/0636, 2015.

Reen, B.: A Brief Guide to Observation Nudging in WRF, Tech. rep., Army Research Laboratory, http://www2.mmm.ucar.edu/wrf/users/docs/ObsNudgingGuide.pdf, 2016.

Sathe, A., Mann, J., Gottschall, J., and Courtney, M. S.: Can Wind Lidars Measure Turbulence?, Journal of Atmospheric and Oceanic Technology, 28, 853–868, doi:10.1175/JTECH-D-10-05004.1, 2011.

Schmehl, R., Noom, M., and van der Vlugt, R.: Traction Power Generation with Tethered Wings, in: Airborne Wind Energy, chap. 2, pp. 23–45, Springer Berlin Heidelberg, Berlin, Heidelberg, doi:10.1007/978-3-642-39965-7_2, 2013.

Skamarock, W. C. and Klemp, J. B.: A time-split nonhydrostatic atmospheric model for weather research and forecasting applications, Journal of Computational Physics, 227, 3465 – 3485, doi:https://doi.org/10.1016/j.jcp.2007.01.037, predicting weather, climate and extreme events, 2008.

Sommerfeld, M., Crawford, C., Monahan, A., and Bastigkeit, I.: LiDAR-based characterization of mid-altitude wind conditions for airborne wind energy systems, Wind Energy, 0, doi:10.1002/we.2343, 2019.

Stauffer, D. R., Seaman, N. L., and Binkowski, F. S.: Use of Four-Dimensional Data Assimilation in a Limited-Area Mesoscale Model Part II: Effects of Data Assimilation within the Planetary Boundary Layer, Monthly Weather Review, 119, 734–754, doi:10.1175/1520-0493(1991)119<0734:UOFDDA>2.0.CO;2, 1991.

Troen, I. and Lundtang Petersen, E.: European Wind Atlas, Risø National Laboratory, 1989.

Upton, G. and Cook, I.: A Dictionary of Statistics, Oxford University Press, 2008.

Wang, W., Bruyère, C., Duda, M., Dudhia, J., Gill, D., Kavulich, M., Keene, K., Lin, H.-C., Michalakes, J., Rizvi, S., Zhang, X., Berner, J., and Smith, K.: ARW Version 3.6 User's Guide, Chapter 7: Objective Analysis (OBSGRID), http://www2.mmm.ucar.edu/wrf/users/docs/user_guide_V3.6/ARWUsersGuideV3.6.1.pdf, 2015.

Witha, B., Hahmann, A., S̃ile, T., Dörenkämper, M., Ezber, Y., García-Bustamante, E., González-Rouco, J. F., Leroy, G., and Navarro, J.: WRF model sensitivity studies and specifications for the NEWA mesoscale wind atlas production runs, Technical report, 73 pages, The NEWA consortium, 2019.